A Rapid, Low-Cost Path to Lunar Communication and Navigation with a Lunar Surface Station

William W. Jun
william.w.jun@jpl.nasa.gov

Toshiki Tanaka
toshiki.tanaka@jpl.nasa.gov

Paul Carter
paul.w.carter@jpl.nasa.gov

Rodney L. Anderson
rodney.l.anderson@jpl.nasa.gov

Sriramya Bhamidipati
sriramya.bhamidipati@jpl.nasa.gov

Kar-Ming Cheung
kar-ming.cheung@jpl.nasa.gov

Jet Propulsion Laboratory
California Institute of Technology
4800 Oak Grove Dr.
Pasadena, CA 91109

Abstract*—Multiple international efforts are developing systems for position, navigation, timing, and communications (PNT+C) for the Moon. These architectures plan to implement a large lunar constellation similar to Earth-like Global Navigation Satellite Systems (GNSS) enabling high-performance PNT+C for a scalable user segment on the lunar surface. However, the collective cost and timeline of a complete infrastructure deployment could reach many billions in USD over decades before surface users can fully utilize its PNT+C capabilities. We propose the use of a lunar surface station to achieve high performance PNT+C for lunar south pole surface users during the initial deployment of a large lunar constellation. The early addition of a single station can provide the same or better PNT+C performance as a large lunar constellation while only requiring a lunar constellation with $\leq$4 orbiters. Thus, a surface-station-enhanced (SSE) PNT+C architecture significantly reduces the required timeline and overall infrastructure cost to achieve accurate and scalable PNT+C. A static lunar surface station positioned at the Connecting Ridge supplies valuable PNT+C services to future missions in nearby permanently shadowed regions. The station provides communication relay and store-and-forward capabilities between lunar relay orbiters and nearby surface users. In addition, the station receives augmented forward signals (AFS) from the LunaNet compatible constellation to generate one-way pseudorange and Doppler shift observables. The station then calculates differential and Joint Doppler and Ranging corrections with these observables and broadcasts corrections, along with an additional AFS, to its surrounding region. Both the corrections and geometric benefits from an additional surface-to-surface AFS result in significant improvements in real-time PNT performance for surface users, even amid large ephemeris and radiometric biases, drift, and noise. With a lunar constellation as small as three orbiters, this SSE PNT+C architecture can achieve $\leq$10 m positioning accuracy (3σ), $<$21 mm/s velocity accuracy (3σ), $<$15 ns timing distribution (3σ), and up to 300 Mbps in data throughput for nearby surface users. Along with PNT+C benefits, the station maintains a highly stable timing reference for time distribution, constellation synchronization, and lunar timekeeping. This paper discusses design considerations for a lunar SSE PNT+C architecture, demonstrates results of simulated PNT and communication performance, and considers extensions of SSE PNT+C architectures to Mars and other planetary bodies. A lunar surface station can enable a rapid path to full PNT+C capabilities, while still providing long-term benefits after the completion of a large lunar infrastructure.

TABLE OF CONTENTS

979-8-3503-5597-0/25/$31.00 ©2025 IEEE

2025 IEEE Aerospace Conference | 979-8-3503-5597-0/25/$31.00 ©2025 IEEE | DOI: 10.1109/AERO63441.2025.11068684

1. INTRODUCTION

There are multiple efforts to develop an interoperable lunar relay network for position, navigation, timing, and communications (PNT+C) on the Moon; these include NASA's Lunar Communications Relay and Navigation Systems (LCRNS) [1], ESA's Moonlight [2], and JAXA's Lunar Navigation Satellite System (LNSS) [3]. These efforts propose a large constellation of lunar orbiters targeting the lunar south pole (LSP), with additional plans for global lunar PNT+C capabilities. The large lunar constellation would mimic Earth's GNSS through the Augmented Forward Signal (AFS) [4], enabling accurate and scalable positioning services for the Moon while also providing communication services through the LunaNet interoperability Specification (Draft V5) (LNIS) [5]. However, deploying 10+ orbiters for a lunar constellation will likely take decades and result in infrastructure costs of billions in USD before users can utilize accurate and scalable PNT+C capabilities. Near term missions, such as the Artemis missions, will still require high-performance PNT+C services during the early deployment of a large lunar constellation; when the number of deployed lunar orbiters ranges from 1 to 3.

Thus, we propose the use of a lunar surface station (SS) to supplement the lunar relay network during its initial phases of deployment and enable accurate and scalable PNT+C services at the LSP. A surface station-enhanced (SSE) PNT+C architecture significantly reduces the cost and timeline for effective PNT+C service deployment. A LunaNet compatible SS located on the LSP utilizing the innovative Joint Doppler and Ranging (JDR) and high-performance clocks enables these PNT+C benefits. The SS estimates JDR corrections on one-way range and Doppler measurements from in-situ lunar orbiters and broadcasts them to lunar users. The SS can also provide communication relay services to nearby users,

resulting in significant increases in data throughput.

Similar SSE architectures exist on Earth, such as differential GNSS (DGNSS) [6], and published literature propose communication towers on the lunar surface [7] [8]. However, this concept's innovations come from its use of JDR and high-performance clocks, use of a sparse navigation infrastructure during the early deployment phases of a lunar relay network, and reduction in overall architecture cost and time to achieve PNT+C services.

JDR is a novel, SSE-based geometric constraint on one-way radiometric measurements that improves on the state-of-the-art by close to a factor of two in estimating real-time user position, velocity, and timing (PVT) [9]. A previous SSE-JDR analysis demonstrated accurate, real-time PVT estimation to $<$10 m at 3σ with a navigation constellation of three satellites, enabling navigation services with a partially complete LCRNS [10]. Another SSE-JDR analysis achieved similar performance ($<$10 m 3σ) for a simulated lunar lander throughout active descent and landing on the LSP [11]. When an SS is available, JDR should be used alongside traditional differential corrections to further improve PNT performance.

Corrections from an SS can aid in PNT, but the crucial components of one-way radiometric systems are the timing and frequency references. If the SS deploys a high-performance clock, it will likely be the best timing and frequency reference on the lunar surface. Thus, the SS's clock could lead the newly established lunar coordinated time. The Jet Propulsion Laboratory (JPL) is actively developing the next generation of high-performance, low-size, weight, and power (SWaP) clocks that can provide timing and frequency references for lunar navigation orbiters and surface assets. These include the Deep Space Atomic Clock (DSAC) and Micro Mercury Trapped Ion Clock (M2TIC), which can achieve 3×10^{-15} and 1×10^{-14} in long-term frequency stability with a SWaP of 9 L / 10 kg / 34 W and 1.1 L / 1.2 kg / 6W, respectively [12] [13]. These clocks, along with other commercially available navigation grade clocks, can enable a lunar timing network that doesn't require frequent synchronization with the Deep Space Network (DSN). Deployment of a high-performance clock on the SS thus reduces the burden on Earth-based infrastructure for lunar PNT+C services.

In addition, the SS can act as a communications relay for nearby surface users. Many proposed lunar relay network constellations assume the use of elliptical lunar frozen orbits (ELFO). These orbiters allow for extended visibility on the LSP at the cost of large distances between the surface and the orbiter. The communications link for a small, autonomous rover on the LSP would benefit significantly with a $<$10 km surface-to-surface link to a nearby SS relay rather than an 8000+ km link to an orbiter.

The applications of SSE PNT+C also extend past the Moon. Due to this system's flexibility with sparse navigation infrastructures, an SSE architecture is directly extensible to the development of PNT+C services on Mars and other planetary bodies (Europa, outer planets, etc.).

This paper first discusses the concept of operations (CONOPS) and the architecture and SS design considerations of a lunar SSE PNT+C architecture. Then, we provide results of simulated PNT performance of multiple user types through a high-fidelity navigation simulation. Next, we discuss communication benefits and data rate capabilities with an SS relay. Finally, we discuss extensions of SSE PNT+C architectures to Mars and other planetary bodies.

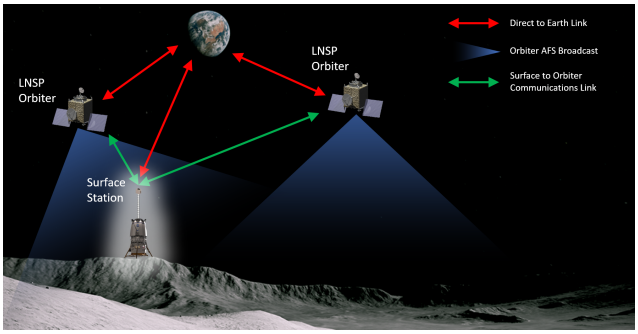

(a) Phase 1: SS Landing and Positioning

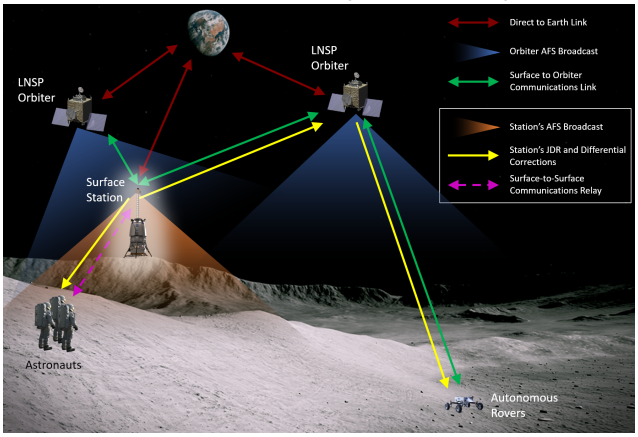

(b) Phase 2: Start of PNT+C Services

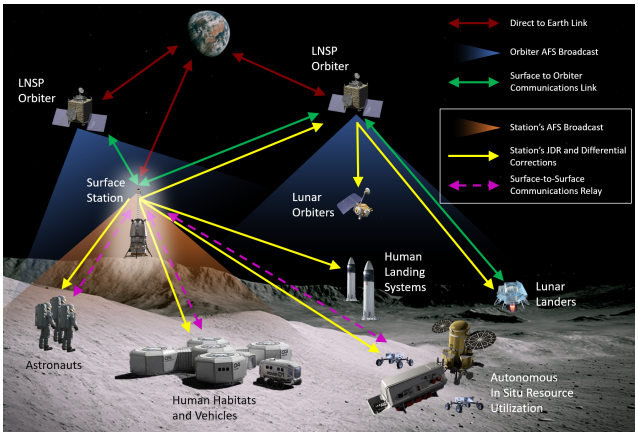

(c) Phase 3: Expanded Operations

Figure 1: CONOPS of an SSE PNT+C architecture on the lunar south pole.

2. SSE PNT+C Concept of Operations

Phase 1: SS Landing and Positioning

The first phase of the CONOPS of a lunar SSE PNT+C architecture begins with an SS landing at the LSP (Figure 1a). A physical realization of an SS can take many forms, ranging from a full mission dedicating a lander to provide SSE PNT+C services to an SSE payload on board a commercial lunar payload services (CLPS) lander.

After successful landing, the SS performs precise positioning

with the LunaNet Service Provider (LNSP) constellation acting as the orbiting navigation and communication nodes. The LNIS allows for point-to-point (P2P) dedicated radiometric measurements as a navigation service separate from the AFS system [5]. The SS can position itself with one or more LNSPs utilizing this P2P service and with additional data such as orbital images or DSN tracking.

An SSE PNT+C architecture is compatible with a constellation of one or more LNSPs; Figure 1a depicts two LNSPs for illustrative purposes. This CONOPS assumes that the LNSPs have already performed orbit determination (OD) before the landing of the SS. This is likely a fair assumption for a lunar use case, but with other planetary bodies such as a Martian SSE architecture, the SS and LNSP constellation can perform joint positioning and OD.

Phase 2: Start of PNT+C Services

Once the SS has precisely estimated its position on the lunar surface, it can begin PNT+C services: phase 2 of the SSE CONOPS. The four major objectives required of the SS are to:

1. Receive LNSP AFS and generate JDR and differential corrections
2. Transmit the calculated corrections to nearby users
3. Broadcast a separate AFS to provide additional radiometric measurements to nearby users
4. Provide communications relay services to nearby users

The SS receives the broadcasted one-way AFS pseudorange code signals from the LNSPs (blue gradients in Figure 1b) and, knowing its precise position and velocity, generates JDR and differential corrections on the AFS pseudorange and Doppler shift measurements [14]. The differential single difference and double difference corrections mitigate shared errors in the radiometric measurements, such as errors in modeled LNSP ephemerides, LNSP clock and frequency errors, propagation errors, and unshared errors such as receiver specific biases [15].

The SS then transmits the correction dataset to the user so that they can perform JDR, single differencing, and double differencing on their respective radiometric measurements. This transmission of data can be done in various ways: the SS can directly transmit the correction data through a surface-to-surface communications link between the station and the user. The SS can also embed the correction data into the navigation message that is modulated onto the SS's own AFS broadcast. However, if the user is not within line-of-sight (LOS) or cannot close a communications link with the SS, the station can also transmit the corrections data though the LunaNet communications network (autonomous rover in Figure 1b). The SS would use an LNSP as a relay, enabling access to the correction data to all users within the coverage of the LNSP constellation, not just within the LOS region of the SS. Finally, the SS can transmit the correction data back to Earth, where operators can use the corrections for post processed navigation estimation of lunar users.

Another function of the SS is to broadcast a separate, one-way AFS pseudorange code signal to its local region (orange gradient in Figure 1b). For user hardware simplicity, the SS's AFS broadcast would maintain the same signal design and transmit frequency as the LNSP AFS, but this may result in unintentional jamming or interference at close distances to the SS. The AFS signal-in-space recommendations provide requirements on minimum and maximum AFS received powers of -166 to -153 dBW [4]. Thus, the SS's AFS transmit power would be designed to maintain these received power requirements in a service volume around the SS, with a minimum and maximum allowable distance from the SS. Another option would be to broadcast the SS's AFS at a different transmit frequency and for users to downconvert to the same baseband frequency as the LNSP AFS; these options are still under investigation.

The final function of the SS is to provide communication relay services to local users. The user segment for communication services do not scale infinitely as with broadcasted pseudorange codes, but the SS can still provide valuable communication services for many users. Data heavy science missions and critical astronaut extravehicular activities (EVA) can reduce their communication hardware requirements by utilizing the SS as a relay for high data rate, surface-to-surface links.

Phase 3: Expanded Operations

The third phase of an SSE PNT+C architecture is expanded operations (Figure 1c). This includes an increased user segment, the use of a larger LNSP constellation, and long-term services like timekeeping and OD.

Assuming now there is a large lunar constellation available, the LNSP constellation itself would be able to provide high-performance navigation services to lunar users. But just as with DGNSS on Earth, an SS can still significantly improve navigation performance with corrections; the JDR and differential corrections from the SS will continue to improve user navigation with a larger constellation.

With one-way broadcasted AFS from the SS and the LNSP constellation, the user segment around the SS can scale in size without a change in quality and availability of the navigation system. The only consideration would be a scaling communication need with an increased user count. Ideally, additional SS's can reduce the communications relay burden on a single SS and increase the coverage for PNT+C services. However, if the number of users in the SS's local region overwhelms the communication capabilities of the SS, some users can fall back on direct-to-orbiter links and accept a lower data rate.

An SSE PNT+C architecture provides significant benefits during the early development and deployment of a large lunar constellation, but SSE will continue to aid and enhance PNT+C services after the full lunar constellation deployment. For instance, the SS can act as an anchor to aid in in-situ orbit determination for the lunar constellation and reduce the burden of tracking on the DSN.

In addition, the SS can perform long-term timekeeping on the Moon with a high-performance clock. The clock onboard the SS will likely be the best clock on the lunar surface, allowing it to lead the lunar coordinated time. The SS can be a centralized hub for time synchronization for both the LNSP constellation and nearby users. For surface users on the LSP, the Earth sets under the lunar horizon for two week intervals resulting in around a 50% availability for LOS access to Earth. For the two weeks without Earth access, surface users on the LSP will have to maintain timing and communications by frequently relaying to the LNSP constellation. An SS with JPL's DSAC can maintain a fractional frequency stability of 3×10^{-15} over 23 days without drift removal [12], thus providing navigation grade timing to all users within the SS's service volume. Thus, with an SSE PNT+C architecture, timing performance at the LSP would no longer be dictated

Table 1: LCNRS SRD simultaneous AFS link requirement and inferred minimum constellation size

	IOC-Alpha	IOC-Bravo		IOC-Charlie
LCRNS Minimum Simultaneous Link Requirement [20]	1 @ 70%	2 @ 70%	3 @ 40%	4 @ 40%
Inferred Minimum Constellation Size	1 LNSP	2 LNSP	3 LNSP	5 LNSP

by the lack of access to Earth.

3. SSE Architecture

Before analyzing the performance of an SSE PNT+C architecture, we must discuss the likely infrastructure available during the early deployment of a lunar relay network. Thus, this work utilizes previous literature and custom analyses to determine a preliminary constellation design, SS position, and SS hardware for a lunar SSE PNT+C architecture.

LunaNet Service Provider (LNSP) Constellation

Proposed Constellation Designs—Public literature provides minimal information about the constellation designs for lunar PNT+C initiatives. However, we can infer a few likely constellation properties. First, many initiatives point towards the use of ELFOs due to their prolonged coverage of the LSP [16]. A wide range of studies have explored the use of frozen elliptical orbits in minimal orbit constellations with applications to navigation and communication at both the Moon and Mars [17] - [19]. With respect to LCRNS, our SSE PNT+C architecture will likely be deployed during the initial operating capability (IOC) phases. NASA's LCRNS Services Requirements Document (SRD) state that the service volumes for the IOC phases mainly focus on the LSP (SV1 and SV2) [20]. Thus, this analysis assumes the use of ELFOs in two orbital planes for all early deployed LNSP orbiters in our lunar constellation.

Next, is the constellation size and deployment timeline. The LCRNS SRD describes minimum constellation sizing requirements (Figure 2) [20]. This requirement states the number of simultaneous links, or LNSPs, that will be available to users on the LSP (SV1) and their coverage duration. Although not explicitly stated, we can infer the number of LNSPs in the constellation from this requirement.

In the IOC-Alpha phase, only one AFS link will be available 70% of the time; this aligns well with the access duration of a single ELFO to the LSP. Next, IOC-Bravo describes an increase to two and three simultaneous AFS links. This increase in links and coverage duration can be explained with a constellation of three LNSPs, so we infer that this phase includes both constellation sizes of two and three LNSP orbiters. Finally, the IOC-Charlie phase describes four simultaneous AFS links in view with the use of LNIS's Lunar Augmented Navigation System (LANS) service. The LANS service provides GNSS-like PNT services to the LSP using a trilateration solution with four or more LNSPs in view. To achieve four simultaneous AFS links 40% of the time, we assume a constellation of five LNSP orbiters, meaning IOC-Charlie includes constellation sizes of four and five LNSPs. The inferred minimum LNSP constellation size during each IOC phase is described in Table 1.

Table 3-3 Minimum Constellation Sizing Requirements

	IOC-Alpha			IOC-Bravo				IOC-Charlie			EOC		
Service Type	Ka-band	S-band	AFS	Ka-band	S-band	AFS		Ka-band	S-band	AFS / LANS	Ka-band	S-band	AFS / LANS
Number of simultaneous links	1	1	1	1	1	2	3	2	2	4	2	2	5
Forward/ Return Link	R only	F+R	F only	F+R	F+R	F only	F only	F+R	F+R	F only	F+R	F+R	F only
Service Volume	SV1			SV1				SV2			SV3		SV3
Min. % Coverage of an Earth Day	70% TBR			75%	90%	70 %	40 %	75%	90%	40% (with max. spatial GDOP<6)	75%	95%	99%

Notes:
-Links from AFS need to provide geometric diversity; LANS is defined by a minimum of four links in view simultaneously from geometrically diverse relays.
-Per requirement LCRNS.3.0030, links for AFS will be ubiquitous for each relay.
-Minimum percent coverage of an Earth Day throughout an active Artemis campaign.

Figure 2: Minimum constellation sizing requirements from LCRNS SRD [20]

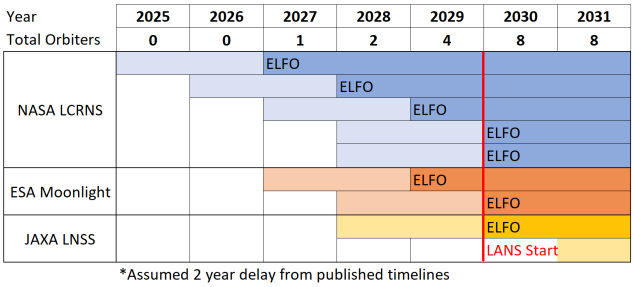

Figure 3: Deployment timelines of LNSP constellations with assumed 2-year delays. Lighter shading indicates published timelines, darker colors include the 2-year delay. Note that the proposed timelines for NASA's LCRNS [20], ESA's Moonlight [21], and JAXA's LNSS [3] were published in 2022 and 2023.

ESA's Moonlight and JAXA's LNSS also propose LNSP orbiters. Moonlight proposes two lunar orbiters in ELFOs deployed in 2027-2028 [21] and JAXA also proposes two ELFOs in 2028 and 2031 [3]. A compiled deployment timeline of LNSP orbiters from all three initiatives is depicted in Figure 3. Note that both the LCRNS SRD and Moonlight documents were published in 2022, and JAXA's in 2023. We assumed a 2 year delay on the deployment of all LNSPs across all initiatives for the sake of this analysis; the delay is not based on any official decisions made by any initiatives.

With the 2 year deployment delay, a minimum LANS AFS service that could provide scalable PNT+C to the LSP would begin at 2030 (requires $\geq$6 LNSPs). Thus, LSP missions up until 2030 will only have partial PNT estimation abilities; they will need to utilize a system such as this SSE architecture if they require accurate and scalable PNT+C services.

Simulated Constellation Design—Knowing that a constellation of four LNSPs before 2030 is the goal determined by this analysis, we designed four sequential LNSP orbit configurations. The four constellation sizes were designed assuming two orbital planes separated by 180 deg in right ascension of ascending node (RAAN). The orbits were first outlined in the Satellite Orbit Analysis Program (SOAP) [22]. The orbital elements of the four constellation configurations are described in Table 2 and they are visualized with their associated access intervals to the LSP in Figure 4.

Assuming only two orbital planes, the three LNSP constel-

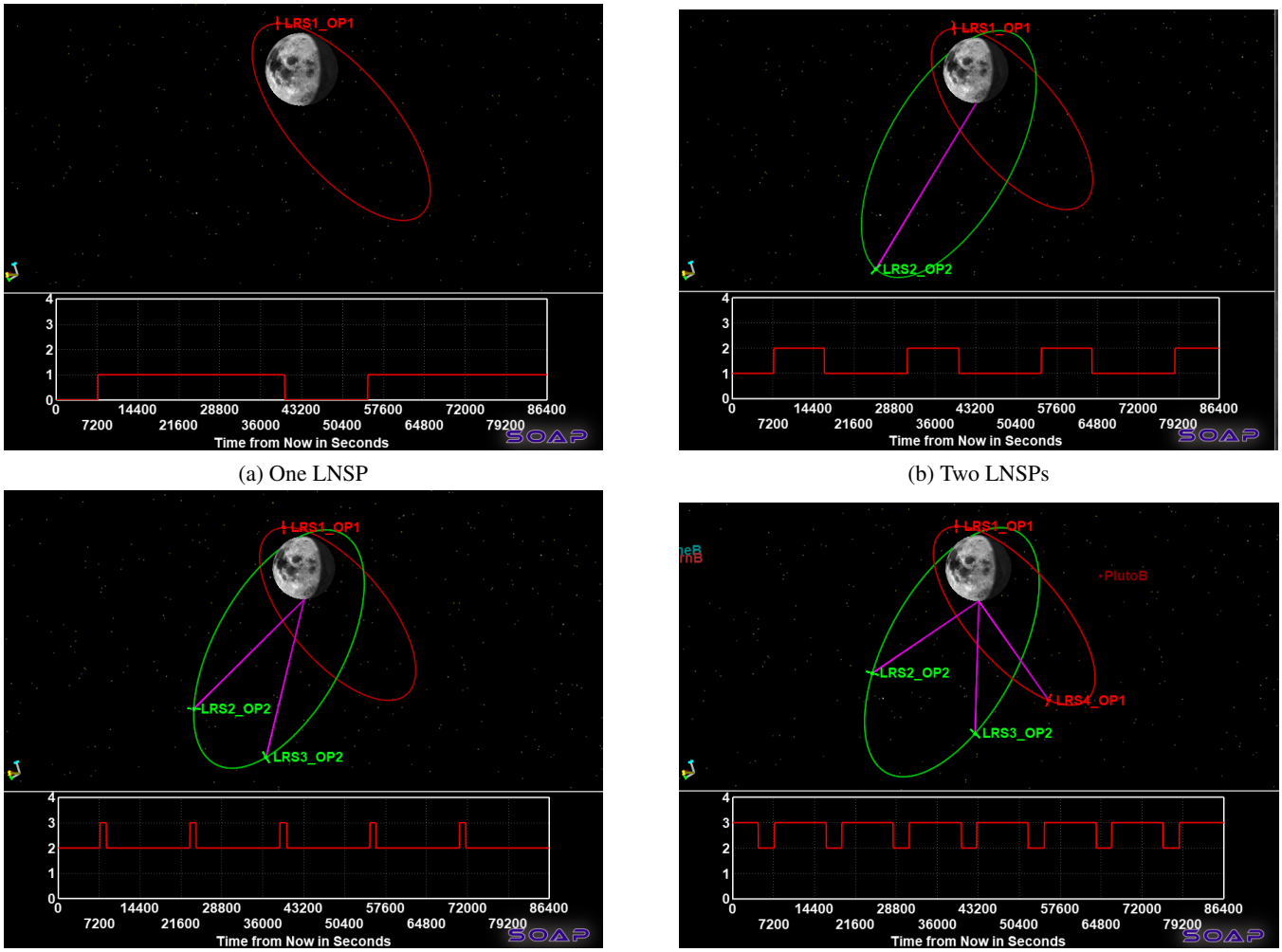

(a) One LNSP

(b) Two LNSPs

(c) Three LNSPs

(d) Four LNSPs

Figure 4: Four LNSP constellation sizes in deployment order with access to the LSP. Screenshots from SOAP. Transitioning between orbit configurations (from size 1-4) only requires changes in orbit anomaly.

Table 2: Orbital elements of four LNSP constellation configurations. Semi major axis, eccentricity, and inclination are the same for all orbits: a = 6541.4 km, e = 0.6, i = 56.2 deg.

Configuration	LNSP	Orbit Plane	RAAN (deg)	ω (deg)	M (deg)
1 LNSP	1	A	0	90	0
2 LNSP	1	A	0	90	0
	2	B	180	90	180
3 LNSP	1	A	0	90	0
	2	B	180	90	120
	3				240
4 LNSP	1	A	0	90	0
	2				180
	3	B	180	90	90
	4				270

lation results in at least two LNSPs in view continuously at the LSP, enabling the use of systems like double differencing. Increasing the constellation size to five LNSPs results in three orbiters continuously in view, and a constellation of six LNSPs results in four orbiters continuously in view enabling standard kinematic trilateration. This analysis only focuses on the first four constellation configurations to depict the benefits of SSE PNT+C during early constellation development.

Once the constellations were roughly designed, we utilized JPL's Monte software [23][24] to propagate the constellation trajectories with higher fidelity. We first generated initial conditions in the IAU Moon pole frame, then integrated in the Earth-Mean Ecliptic 2000 frame. The analysis used the DIVA integrator, which has been used at JPL since the 1970s, including Sun, Earth, and Moon gravity perturbations [25][26]. Propagation of the LNSPs utilized the DE440 ephemeris, which includes JPL precise positions for all the planets [27]. Monte generated orbits for all configurations over a period of one year, and directly generated binary SPICE files for use in subsequent simulations. In each configuration, the two elliptical orbit planes were found to remain stable under Earth and Sun perturbations. The transitions between constellation configurations given realistic propellant budgets and time

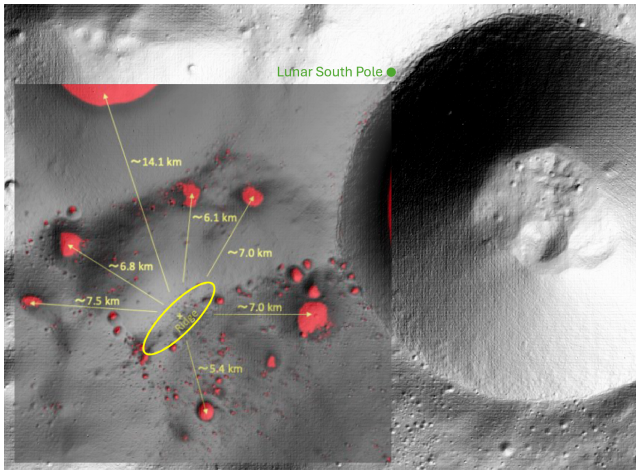

Figure 5: LSP DEM in QGIS with an overlaid map of LSP PSRs [28]. The yellow ellipse indicates the Connecting Ridge and the green circle is the lunar south pole.

constraints will be studied in future work.

Lunar Surface Station

Next, this work analyzed potential sites for the SS. To determine the optimal location, we performed LOS coverage analyses to maximize coverage area with permanently shadowed regions (PSR) in the LSP; these will be prime science and resource targets for future missions. The LOS coverage of the SS is especially important for the SS's AFS broadcast. However, communications may still be possible over the horizon with diffraction effects around terrain. Thus, we also perform a radio frequency (RF) analysis to determine received power in the SS's service volume.

LOS Coverage Analysis—The SS should be located on a site that maximizes PNT+C service availability for the LSP. Thus, this work performed a LOS coverage area analysis for various sites on the LSP. As a starting point, we selected the Connecting Ridge (CR) as the search space for the potential SS site due to its relevance to lunar science and high illumination conditions [28]. The CR runs between the Shackleton and De Gerlache crater, and it is situated on the top of a ridge that connects the two craters (Figure 5). The CR will likely be a key region for exploration missions for two reasons: first, it provides great access to multiple PSRs, which are of the highest scientific interest. Figure 5 shows the locations of PSRs near the CR. Second, the CR receives sunlight for more than 70% of the time on average, which can mitigate power management issues [28]. We assume the SS is located within or near the CR and provides PNT+C coverage to the surrounding area within a range of up to a few kilometers, including PSRs.

The performance of the SS, particularly the range and coverage of RF signals, is subject to the topology of the lunar surface around the SS. Thus, this work utilized a 5 m resolution digital elevation map (DEM) of the LSP produced by the Lunar Reconnaissance Orbiter's Lunar Orbiter Laser Altimeter (LOLA) [29]. This DEM was fed into QGIS, an open source geographic information software, to perform the analysis [30]. QGIS has a built-in function called viewshed to calculate LOS coverage. The viewshed analysis takes into account the topology of the DEM as well as inputs including the height of the transmitting antenna, height of the receiving

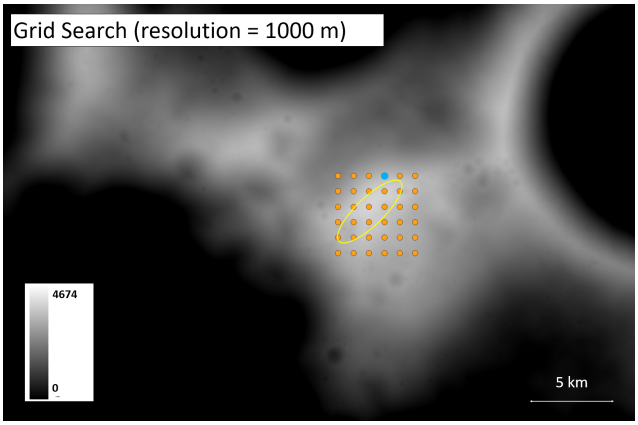

(a) SS grid search

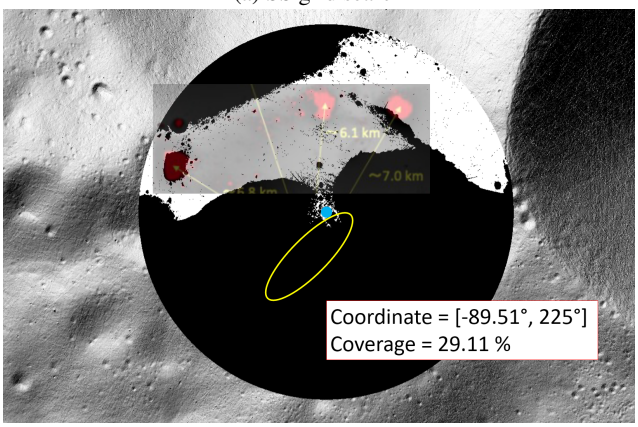

(b) LOS coverage

Figure 6: (a) QGIS-based grid search for SS location on the CR and site with the largest LOS coverage. (b) LOS coverage area overlaid with PSR map [28].

antenna, and the size of the area to be analyzed to calculate the area percentage around the SS that has direct LOS to the transmitter (Figure 6).

Based on the viewshed plug-in, we developed a custom Python workflow connected with QGIS that can compare LOS coverage of multiple points specified by the user, based on user-defined metrics. In this workflow, a Python script creates a grid of SS locations to evaluate, calculates the LOS area percentage for each location in QGIS, and outputs the site with the best coverage. The resolution of the grid search space began at 1 km (between points) and reduced to 100 m to obtain more granular results. In these coverage analyses, the height of the transmitting antenna on the SS was assumed to be 15 m off the surface, and the receiving antenna on a rover at 2 m. The radial distance for the coverage analysis was set at 8 km. Figure 6a depicts an altitude-based visualization of the CR overlaid with an illustrative grid at a 1 km resolution. The visualization indicates that the CR is at the top of a ridge with gradual slopes in all directions. Figure 6b depicts an output of QGIS: a binary map of the site with a large LOS coverage.

This work performed multiple coverage analyses for various optimization parameters. One option was to consider the site in the CR with the highest altitude. However, this site was found to have relatively low LOS coverage area due to local topographical features that would block LOS. Additional analyses suggested that locating the SS at the upper rim facing

the PSRs would be more advantageous. Thus, the chosen SS site (-89.51°,225°) did not have the largest LOS coverage area, but was selected because it provides a wide coverage to the upper region of the SS that includes two PSRs and partially covers one more (Figure 6b).

RF Propagation Analysis— Once an SS site was selected, we utilized Altair's FEKO, a high-frequency electromagnetic simulation software [31], for the RF propagation analysis. With some basic RF hardware assumptions on the SS and a receiving rover, FEKO generated RF path loss maps of the SS transmitter. We assumed antenna heights of 15 m for the transmitter and 2 m for the receiver, an omnidirectional antenna for the transmitter, and a transmit frequency of UHF (442.5 MHz) or S-Band (2245 MHz). To measure path performance, the SS transmitter (TX) power is set to 0 dBm, TX antenna gain at 0 dBi, and receiver (RX) antenna gain at 0 dBi. FEKO calculates propagation using a deterministic two ray model in LOS areas, and using knife edge diffraction for areas without LOS.

If one overlays the LOS coverage map from Figure 6b onto the RF propagation maps in Figure 7, one will notice that the RF propagation exceeds the LOS limits of the SS. Some regions near the SS without direct LOS have reasonable path loss levels through diffraction, at which the rover should be able to close the communication link with an appropriate transmitter and receiver. This effect is more prevalent with the lower band UHF. These regions without direct LOS but with enough RF power to close a communications link would still be able to utilize most PNT+C services from the SS, but with delays in the SS's AFS broadcast due to diffraction effects.

Hardware and Functionality— Next, we discuss the various functionalities that an SS would require to achieve the four objectives described in the CONOPS section. Table 3 summarizes the technology readiness levels (TRL) and mass estimates of each functionality. Note that the mass estimates are relative to a large, dedicated SS lander such as described in [7]. A payload version of the SS in a CLPS mission may have reduced mass estimates and functionalities. Almost all functionalities of the SS can leverage existing technologies with high TRL, with the exception of the deployable communications structure and some LNIS functions. These technologies currently have moderate TRLs and are awaiting further demonstrations. The following sections describe each functionality and potential hardware choices on the SS.

Transponder: The mass and power consumption of the communication systems, including transponder and antenna, was estimated based on the COMPASS Lunar Communications Tower (LCT) design report [7]. In the COMPASS LCT study, a mass of 100 kg and a power consumption of 288 W were assumed to support Ka-band bi-directional links to LNSPs and for direct to Earth. This configuration also supports 2 x 100 Mbps return, S-band bi-directional links to LNSPs and for direct to Earth, as well as 802.16 WiMax-based surface communication with a data rate of up to 80 Mbps.

These mass and power values correspond to a tower-based communications system on a large lander dedicated to the objectives of an SSE PNT+C system. Smaller mass and power requirements may be possible with other SS configurations, such as through an SSE CLPS payload or a payload on the lander component of an autonomous rover.

Deployable Communications Structure: Direct LOS between the SS and a user provides the maximum utilization of SS

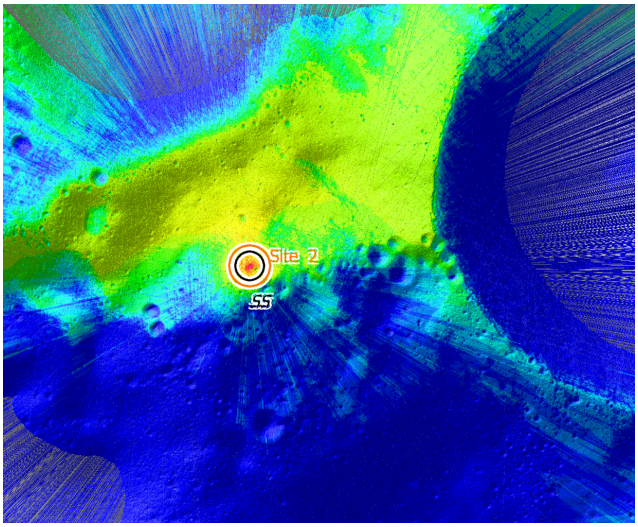

(a) UHF (442.5 MHz)

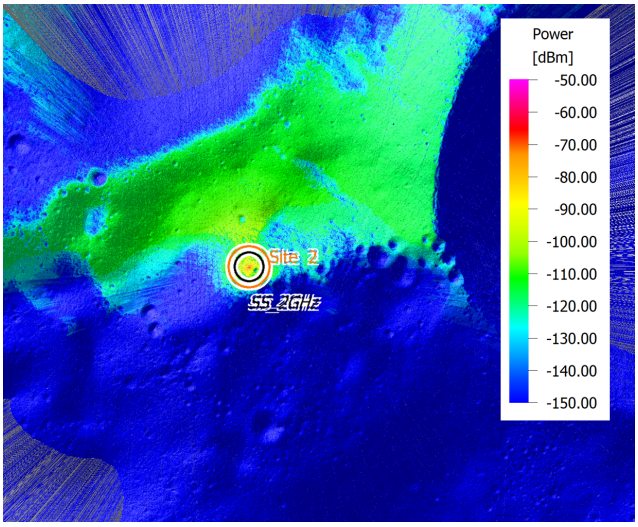

(b) S Band (2245 MHz)

Figure 7: FEKO generated RF propagation maps with an SS transmitting at either UHF or S Band. The power values depict path loss; TX power, TX antenna gain, and RX antenna gain are all 0 dBm and 0 dBi. TX antenna height is 15 m and RX antenna height is 2 m.

benefits. Thus, to increase direct LOS coverage, the SS's antenna should maximize its height off the surface. Currently, the best option for raising the altitude of the SS antenna is through a deployable structure. The deploying mechanism will need to be reliable and mitigate single-point failures. Some studies on deployable structures even require the mechanism to be retractable for reversibility.

The COMPASS LCT assumed a 10 m deployable boom weighing 20.7 kg including a 15% margin [7]. More recently, Honeybee Robotics is developing a 14-m deployable boom designed for solar panel deployment on the lunar surface, known as the Lunar Array, Mast, and Power System (LAMPS) [32] (Figure 8). LAMPS achieved a TRL of 5 in 2023 and is now aiming to reach TRL 6 within the next two years through additional technical demonstrations. Another recent study by the Massachusetts Institute of Technology (MIT) examined a 16.5-m deployable boom designed to

Table 3: Functionalities of the SS with their associated SS objective, TRL, and mass estimates. The mass estimates are relative to a large, dedicated SS lander such as in [7]. A payload version of the SS in a CLPS mission may have reduced mass estimates and functionalities. The acronyms are range and range-rate (RARR) and delta-differential one-way ranging (DDOR).

Functionalities of the Surface Station			Objective	TRL	Mass
Transponder	Direct to LNSP communication	Receive and process LNSP AFS broadcast	1	Mid	100 kg
		Relay communications to/from LNSP	2, 4	High	
		Time-transfer from LNSP	3, 4	High	
	Direct to Earth communication	RARR & DDOR with Earth ground station	1, 3	High	
		Relay communications to/from Earth	4	High	
		Time-transfer from Earth ground station	3, 4	High	
	Surface communication	AFS broadcast to surface users	3	Mid	
		Correction broadcast to surface users	2	Mid	
		Communication relay services	4	High	
High stability clock			3	High	10 kg
Communication tower deployable structure			1, 2	Mid	20 kg
Power and thermal control			1, 2, 3, 4	High	3 - 45 kg

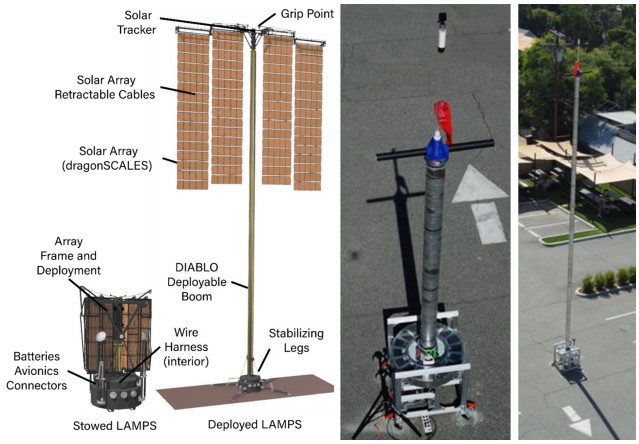

Figure 8: LAMPS developed by Honeybee Robotics in partnership with mPower Technology [32]. Left is a concept illustration of LAMPS and right is a prototype test deployment.

elevate a 1U CubeSat payload package, called the Multi-functional Expandable Lunar Lightweight and Tall Tower (MELLTT) (Figure 9). MELLTT achieved a TRL of 3-4 in 2023 after demonstrating the hardware on the ground [33].

For our research, we assume a deployable boom with the SS's antenna 15 m from the lunar surface. Although the current TRL of these deployable structures is around 5, ongoing research programs are expected to increment the TRL. The mass of the tower architecture is assumed to be 20 kg based on the LCT design, but it could be changed depending on technology needs and SWaP requirements.

As stated before, LSP users do not require direct LOS with the SS. Differential and JDR corrections can be transmitted from the station directly to the user over the horizon or broadcasted to an LNSP which would relay them to users. However, direct LOS with the station guarantees the additional AFS range code from the SS, which can provide significant benefits in PNT geometric diversity, and improves surface-to-surface communication capabilities.

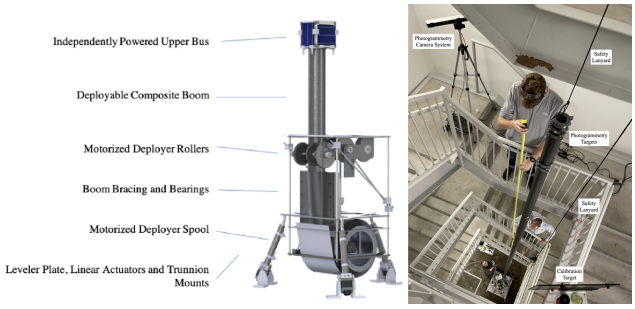

Figure 9: MELLTT developed by MIT [33]. Left is a concept illustration of MELLTT and right is a prototype test deployment.

Power and Thermal Control: Current solutions for power on the LSP include solar arrays and radioisotope thermoelectric generators (RTG). Previous literature has performed studies of power solutions of a lunar SS and their considerations with different SS concepts [8]. Lack of continuous sunlight and thermal considerations make RTGs an attractive option. A lunar day/night cycle is approximately 29.5 Earth days (708 hours), resulting in a lunar day equivalent to about 14.75 days (354 hours), with the same duration for the lunar night; the 14.75-day lunar night is a worst-case scenario [34]. Depending on the location in the LSP, increasing the height of solar panel structures can reduce the night cycle to as little as 100 hours [8]. These lunar day/night cycles result in large temperature fluctuations from 75 K - 300 K in the LSP [34].

RTGs can provide continuous power for decades, far exceeding the lifespan of typical batteries or the duration that solar panels can be effective, especially in environments with limited sunlight. Additionally, the heat generated by RTGs can be used to keep spacecraft instruments warm, ensuring they operate correctly in the extreme cold of space or on distant planetary surfaces. RTGs are an established technology which have been used for many planetary missions, such as Voyager 1 and 2, New Horizons, Cassini-Huygens, and the Curiosity and Perseverance rovers. A state-of-the-art, Multi-Mission Radioisotope Thermoelectric Generator (MMRTG) powers the Martian rovers [35] (Figure 10). These MMRTGs are around 66 cm tall, have a fin-tip to fin-tip

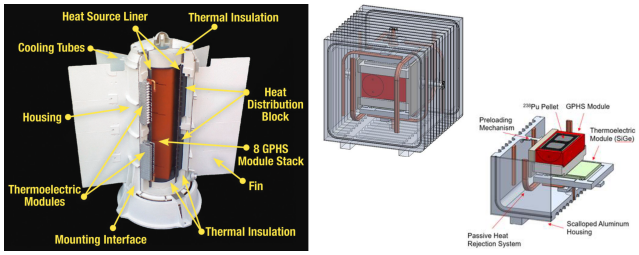

Figure 10: RTG options for power and thermal control on the SS. Left: MMRTG [35] and right: SLP-RTG [36].

diameter of around 64 cm, and weigh around 45 kg. They produce around 110 watts of electrical power and 2,000 watts of thermal power at launch [35]. Advancements in RTGs technologies could enable small-SWaP RTGs. These conceptual small, low-power radioisotope thermoelectric generators (SLP-RTG) could provide 10s of watts of electrical power and 100s of watts of thermal power at a size of approximately 25 cm x 25 cm x 25 cm and an anticipated mass of 3 kg at under $10M[2] (FY2024) [36] (Figure 10). These small-SWaP RTGs could enable the use of a long-term SSE payload on a CLPS lander instead of a large, dedicated SS.

High Stability Clocks: Due to the lack of Earth access for around two week intervals at the LSP, timing references need to maintain stability throughout these long periods independent of signals from Earth. The generation and broadcast of an AFS requires high timing accuracy and stability, meaning autonomous and long-term stable (low drift) atomic clocks are essential for precise lunar navigation.

The current state-of-the-art for deep space clocks is the DSAC [12]: JPL's latest demonstrated advancement in trapped ion atomic clocks (Figure 11). During its 2-year technology demonstration in space, DSAC demonstrated a short-term stability of $1.5 \times 10^{-13}/\tau^{1/2}$ and a long-term stability of 3×10^{-15} over 23 days; a time deviation of only 4 ns at 23 days with no drift removal. For other SS realizations, such as with an SSE payload, timing options include the low-SWaP Micro Mercury Trapped Ion Clock (M2TIC) [13]. M2TIC prototypes can reach 1×10^{-14} at 1 day, but with a significantly reduced SWaP of 1.1 L, 1.2 kg, and under 6 W (Figure 11).

These clocks, along with other commercially available atomic clocks, can enable an SS to provide long-term stable timing references for PNT services, time distribution to LNSPs and users, and lunar timekeeping.

Lunar Surface Users

Finally, this work generated trajectories for various surface users. We focused on two user types ranging in speed and behavior: an autonomous rover performing a sweep of a PSR and a crewed vehicle circling a PSR.

To generate user trajectories, we modified the Python and QGIS workflow developed for the LOS coverage analysis. The inputs to the workflow include motion rules, trajectory length, and other constraints. This workflow generates trajectories in CSV format, producing latitude, longitude, and

[2]The cost information contained in this document is of a budgetary and planning nature and is intended for informational purposes only. It does not constitute a commitment on the part of JPL and/or Caltech.

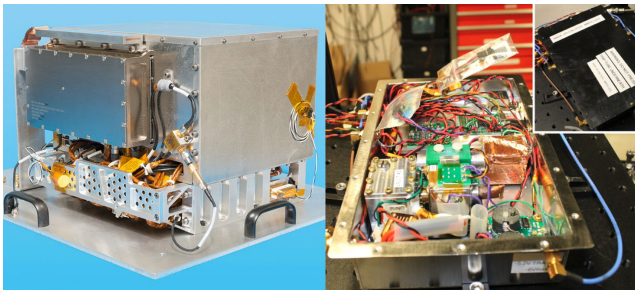

Figure 11: Highly stable clock options for time and frequency references on the SS. Left: DSAC [12] and right: M2TIC prototype [13].

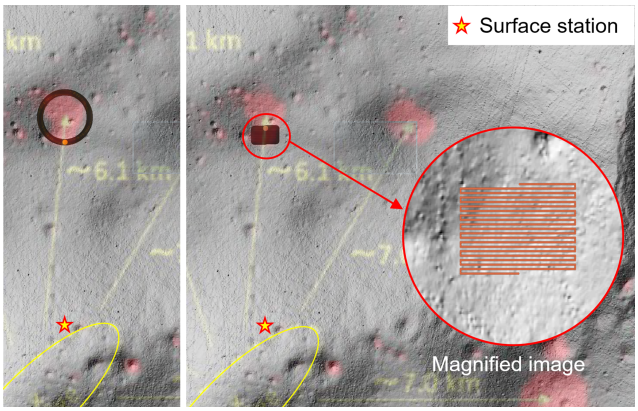

Figure 12: LSP user trajectories generated by the Python QGIS workflow. Left: circular trajectory around a PSR by a crewed lunar vehicle and right: grid trajectory in a PSR by an autonomous ISRU rover.

altitude of the user at sequential timesteps in addition to the SS-to-user direct LOS access. Because the DEM imported into QGIS is limited to a 5 m resolution, an additional step after the Python workflow was to interpolate the user trajectory to a finer resolution, also providing control over velocity of the trajectory.

The first user type is a crewed lunar vehicle. This vehicle drives in a circular path around the PSR, exploring and scouting the region. The second user type consists of an in-situ resource utilization (ISRU) mission led by an autonomous rover. This rover explores or harvests resources in a PSR near the LSP. Both trajectories are approximated in Figure 12. After interpolation, these user trajectories have largely varying speed magnitudes; Figure 13 depicts user speed per axis for each user type. Because the user trajectory generation workflow utilized the DEM in QGIS, the trajectory position and velocities vary over time with local terrain.

4. Navigation and Timing Performance

Navigation Simulation

To evaluate the navigation performance of the SSE PNT+C architecture, this work implemented a high-fidelity navigation simulation in MATLAB. This analysis utilized the same navigation simulation from previous JDR analyses [10] [14], but with the LNSP constellation, SS, and user trajectories described in the previous section. The simulation assumes bias, drift, and noise on the modeled orbit ephemerides,

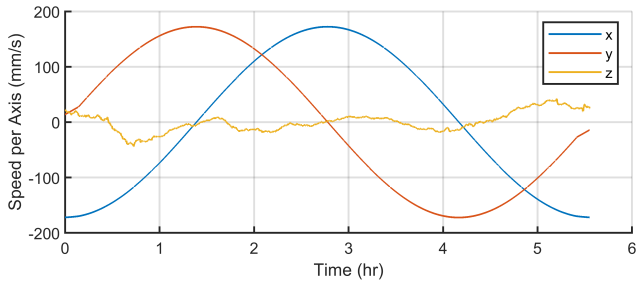

(a) Crewed vehicle: circle trajectory

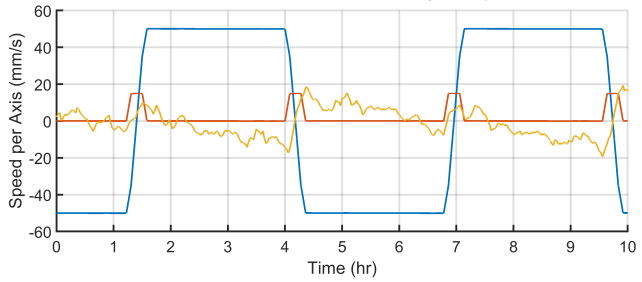

(b) Autonomous ISRU rover: grid trajectory

Figure 13: Per axis speed of both crewed vehicle and autonomous rover user trajectories. Note that the duration of both trajectories are different due to user speed. Axes are in the lunar inertial reference frame.

Table 4: DLL and FLL tracking loop parameters. Some values taken from [37]

Parameter		Value
Chip Length	λ_C	29.305 m
Loop Bandwidth	B_L	1 Hz
Early-Late Spacing	d	1 chip
Integration Time	T	1 sec
Factor	F	1 (high C/N_0)

SS position and velocity, and in radiometric measurements. The modeled errors on the radiometric measurements are derived from tracking loop thermal noise, propagation errors, and an oscillator phase noise model dependent on the clock deployed at each navigation node; more detail on error generation is described in previous papers [14]. This analysis does not fully simulate the delay locked loops (DLL) and frequency locked loops (FLL) assumed for the pseudorange and Doppler measurements, but instead models their thermal noise and dynamic stress. An updated thermal noise model scales based on the carrier to noise power (C/N_0) simulated for each link [38]:

$$\sigma_{tDLL} = \lambda_C \sqrt{\frac{B_L d}{2C/N_0}\left(1 + \frac{1}{TC/N_0}\right)} \quad (m) \qquad (1)$$

$$\sigma_{tFLL} = \frac{1}{2\pi T}\sqrt{\frac{4FB_L}{C/N_0}\left(1 + \frac{1}{TC/N_0}\right)} \quad (Hz) \qquad (2)$$

where the parameters are described in Table 4. The C/N_0 is simulated with user hardware assumptions similar to the astronaut EVA suit described in section 5 and the orbiter transmitter in [37]. The dynamic stress errors are incorporated into the simulated noise for both FLL and DLL [14] [37].

Table 5: Bias value scaled by a uniform random distribution, drift rate 1σ, and Gaussian noise 1σ of simulated measurements and user knowledge.

	Uniform Bias		Drift Rate 1σ		Noise 1σ	
Pseudorange	δt_{USR}	5000 ns	$\dot{\delta t}_{USR}$	10 ns/hr	$w_{\delta t_{USR}}$	5 ns
	δt_{SS}	0 ns	$\dot{\delta t}_{SS}$	4 ns/23 days	$w_{\delta t_{SS}}$	1 ns
	δt_{LNSP}	1 ns	$\dot{\delta t}_{LNSP}$	4 ns/23 days	$w_{\delta t_{LNSP}}$	1 ns
					$\varepsilon_{\rho_{LNSP}}$	1 m
					w_ρ	1 m
LNSP	$\vec{b}_{S_r,radial}$	1 m	$\dot{\vec{b}}_{S_r,radial}$	0.1 m/hr		
	$\vec{b}_{S_r,along}$	10 m	$\dot{\vec{b}}_{S_r,along}$	1 m/hr		
	$\vec{b}_{S_r,cross}$	10 m	$\dot{\vec{b}}_{S_r,cross}$	1 m/hr		
	$\vec{b}_{S_v,radial}$	1 mm/s	$\dot{\vec{b}}_{S_v,radial}$	1 mm/s/hr		
	$\vec{b}_{S_v,along}$	10 mm/s	$\dot{\vec{b}}_{S_v,along}$	10 mm/s/hr		
	$\vec{b}_{S_v,cross}$	1 mm/s	$\dot{\vec{b}}_{S_v,cross}$	1 mm/s/hr		
SS	$\vec{b}_{R_r,xyz}$	1 m	$\dot{\vec{b}}_{R_r,xyz}$	10 mm/hr		
	$\vec{b}_{R_v,xyz}$	1 mm/s	$\dot{\vec{b}}_{R_v,xyz}$	0.01 mm/s/hr		

Table 6: Doppler frequency measurement error parameters [10]. The user deploys a chip scale atomic clock and the SS deploys a DSAC. AeB signifies $A \times 10^B$

Oscillator		CSAC	DSAC
Error	Statistic	**User**	**Surface Station**
$b_{osc,S}$	$b_{osc,t}$	0 Hz	0 Hz
$b_{osc,X,R}$	$b_{osc,r}$	$\pm$3e-10f_0 Hz	0 Hz
$w_{prop,k}$	b_{prop}	$\pm$0.01 Hz	$\pm$0.001 Hz
$\dot{b}_{S,k}$	$\sigma_{\dot{b}_t}$	2.29e-8 Hz/hr	2.29e-8 Hz/hr
$\dot{b}_{X,R,k}$	$\sigma_{\dot{b}_r}$	2.29e-5 Hz/hr	2.29e-8 Hz/hr
$w_{\Delta f^{FLL}_{X,R,k}}$	σ_{FLL}	$\sigma^X_{tFLL,k} + f^X_{e,k}/3$	$\sigma^R_{tFLL,k} + f^R_{e,k}/3$
$w_{b_{osc,S,k}}$	$\sigma_{osc,t}$	8.99e-7 Hz	8.99e-7 Hz
$w_{b_{osc,X,R,k}}$	$\sigma_{osc,r}$	0.0172 Hz	8.99e-7 Hz
$w_{prop,k}$	σ_{prop}	0.01 Hz	0.001 Hz

Table 5 and 6 describe the updated error parameters utilized in this navigation simulation. As with previous analyses, radiometric errors are unique to each link; the errors on the links between all LNSPs, the SS, and the user are independently simulated and combined during each transmitter / receiver measurement realization. Thus, errors from a single LNSP that are shared in radiometric links to both the user and the SS can be mitigated through JDR and differential corrections. Double differencing further mitigates receiver specific errors onboard the user and SS. The simulated frequency biases on the user receiver's Doppler shift measurement can be up to 1 Hz, resulting in significant errors for methods that cannot utilize double differencing's Doppler bias mitigation. Although the user's clock bias is estimated, the Doppler biases are not and can only be diminished through double differencing methods and/or calibration.

The simulated user deploys an extended Kalman filter (EKF) to estimate a 7 element state in real-time: 3D position, 3D velocity, and a user clock bias, assuming a range and Doppler measurement from each LNSP in view at each second. If the user has access to 2 or more LNSPs the EKF automatically

utilizes double differencing (DD). If there is access to only one LNSP, the EKF reverts to single differencing (SD). With no LNSP access, the user can only navigate with the surface-to-surface pseudorange measurement broadcast through AFS from the SS. We do not simulate any inertial navigation systems so that the results directly compare the performance of the SSE and non-SSE PNT systems.

A moving user estimating 7 dynamic states with a constellation of only one LNSP results in an unobservable solution. Thus, for the single LNSP constellation, this analysis assumes a static user. For constellation sizes 2 - 4, the analysis simulates navigation performance for both the crewed vehicle and autonomous rover users. In the two LNSP constellation there are intervals with only one LNSP in view. During these intervals the user stops moving; the user resumes its trajectory when two LNSPs are available.

This analysis evaluates three different navigation methods: traditional range and Doppler (Trad RD), traditional DD (Trad DD), and DD with JDR (DDJDR). Trad RD creates a baseline for PNT performance without an SS. The double differencing methods benefit most from an SSE PNT+C architecture, but DDJDR increments on Trad DD with the innovative JDR. Thus, DDJDR is the default navigation method used with SSE when two or more LNSPs are in view to a user. Figures 17 - 19 at the end of this paper provide the distribution of performance of all navigation methods for PVT estimation of both user types.

The navigation simulation begins with a process noise optimization to achieve the best simulated performance. This analysis optimizes for position estimation accuracy, but the process noise can be changed to optimize for velocity or timing estimation. The analysis then begins a Monte Carlo simulation with 1000 iterations using the optimal process noise values for each method.

Results— Figure 14 depicts the mean and 3σ root-sum-squared (RSS) PVT error over the entire analysis interval for the crewed vehicle user and a three LNSP orbiter constellation. The figure compares the use of DDJDR with the traditional DD method, depicting the improvements in position estimation stability with JDR relative to the state-of-the-art. Both methods converge to under 20 m within the first few minutes, and both mean errors steady state to under 5 m. However, DDJDR provides a more stable positioning solution throughout challenging geometry scenarios, resulting in a lower overall 3σ positioning error. A similar result is shown in timing performance, while velocity estimation is near identical between both methods.

When comparing the steady state performance of the two methods ($>$2 hours), DDJDR achieves a RSS 3σ positioning performance of 10.0 m, more than a 60% improvement on Trad DD's 16.3 m at 3σ. Thus, DDJDR, the default SSE-JDR method, improves on traditional DD with no changes in architecture and no additional measurements. Even more, due to the significant radiometric errors (such as Doppler biases), SSE-JDR improves on non SSE methods (Trad RD) by near an order of magnitude (Figure 15). With varying constellation sizes, the SSE-JDR navigation system consistently provides order of magnitude improvements in position estimation accuracy relative to Trad RD (Figure 17).

Table 7 depicts the 3σ PVT performance of the SSE-JDR system with respect to constellation size. It is clear that additional orbiters improve performance: there is an order

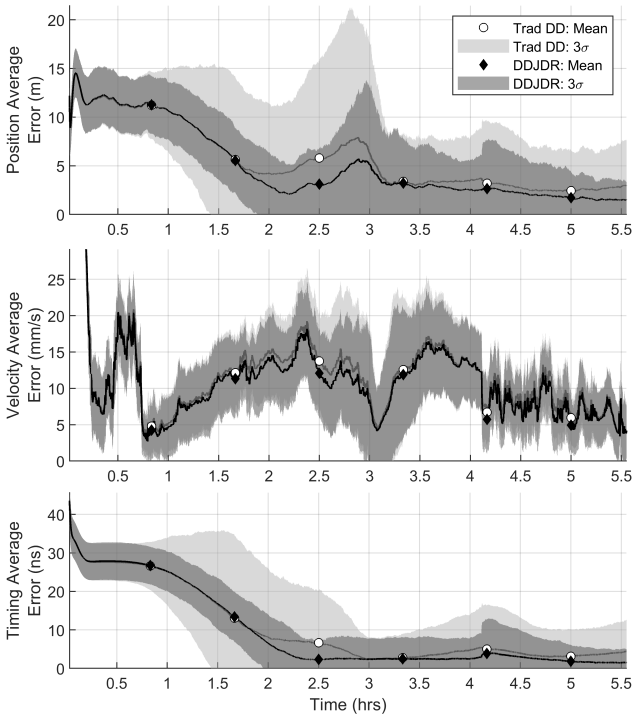

Figure 14: Mean and 3σ PVT error for DDJDR and Trad DD for the crewed vehicle and a 3 LNSP constellation over 1000 simulations. Throughout the entire analysis interval the LSP has access to two LNSPs with two short intervals ($\sim$10 min) with access to all three LNSPs.

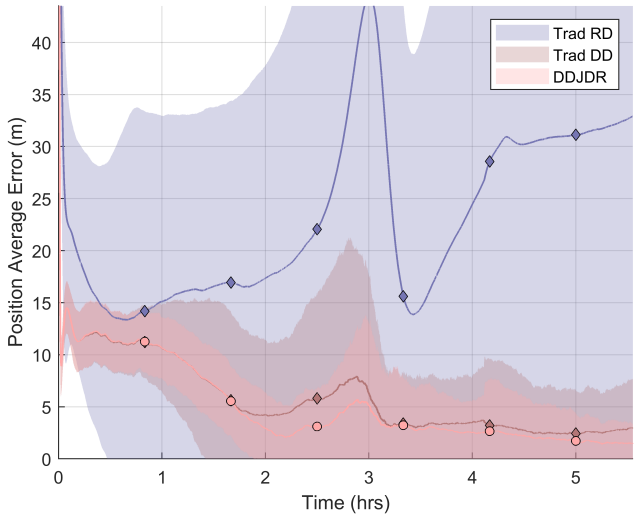

Figure 15: Mean and 3σ positioning error showing near order of magnitude improvement between traditional range and Doppler vs. double differencing methods for the crewed vehicle and a 3 LNSP constellation over 1000 simulations.

Table 7: 3σ (99.73%) confidence of state estimate error over 1000 simulations for crewed vehicle, autonomous rover, and static user over all constellation sizes for DDJDR. The values (X, Y) are X for mean and Y for standard deviation of error.

	LNSP Count	2	3	4
Crewed Vehicle	Pos (m)	21.6 (8.8, 3.8)	10.0 (2.7, 1.3)	5.6 (1.7, 0.8)
	Vel (mm/s)	108.3 (53.9, 16.2)	20.6 (10.3, 1.9)	17.5 (5.9, 1.9)
	Clk (ns)	13.9 (3.4, 0.3)	10.9 (0.8, 0.6)	5.9 (0.4, 0.3)
Autonmous Rover	Pos (m)	20.0 (6.2, 3.5)	9.0 (2.1, 1.0)	6.6 (1.9, 1.0)
	Vel (mm/s)	89.0 (33.1, 11.7)	17.9 (5.1, 2.4)	12.8 (2.9, 1.0)
	Clk (ns)	35.8 (1.8, 1.3)	14.1 (0.7, 0.5)	9.3 (0.6, 0.4)
	LNSP Count	1		
Static User	Pos (m)	13.9 (5.0, 2.3)		
	Clk (ns)	25.6 (2.3, 1.6)		

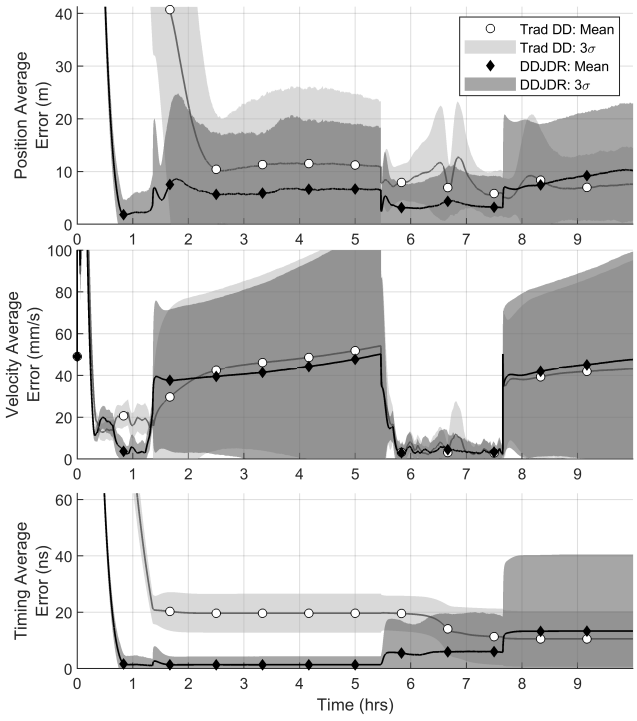

Figure 16: Mean and 3σ PVT error for DDJDR and Trad DD for the autonomous rover and a 2 LNSP constellation over 1000 simulations. This analysis interval begins with access to two LNSPs at the LSP until 1.3 hrs, then access reduces to only one LNSP in view until 5.5 hrs. This cycle of two and one LNSP access repeats until the end of the analysis interval. Double differencing is only possible with ≥ 2 LNSPs in view; with access to only 1 LNSP, DDJDR falls back to single differencing with JDR.

of magnitude improvement with the increase from two to four LNSPs. This is as expected, due to the two orbiter constellation containing intervals of only one LNSP in view. This forces the user to utilize single differencing techniques instead of double differencing, no longer mitigating user frequency biases. These effects can be seen in Figure 16, where intervals with two LNSPs in view result in sub-20 m 3σ performance, but the overall 3σ performance is degraded by intervals with only one LNSP in view. In addition, the time to convergence takes longer with fewer LNSPs in view.

Ultimately, the SSE PNT+C system can provide significantly improved, real-time PVT estimation for users in the LSP. The addition of an SS at the LSP that can provide PNT services enables order of magnitude improvements in positioning performance with only a fraction of the orbiters planned for a full lunar constellation. With only three LNSPs, the SSE-JDR method can achieve LCRNS SRD's position knowledge requirement of 10 m (3σ) [20].

5. Communication Performance

In addition to improving PNT performance during the early stages of lunar relay constellation deployment, the SS can also provide communication advantages to users in the LSP. As a critical piece of lunar infrastructure, the SS will likely be equipped with a large, high-power antenna and radio system, and will also be orders of magnitude closer to the surface users than any LNSP orbiters. By communicating through the capable SS, rather than directly to relays or to Earth ground stations, users can simultaneously improve their potential data return and relax SWaP requirements for their telecommunication subsystems.

To quantify the communications benefits of the SS, this research performed a basic link analysis with two candidate lunar surface users: an astronaut wearing an EVA suit and an autonomous rover. The telecommunication hardware and link assumptions for the SS, LNSPs, Earth ground station, and users are summarized in Table 8. The link analysis accounts for basic losses and noise sources appropriate for each link. For links from the lunar surface to LNSP relays, the only loss considered (in addition to the assumed hardware losses listed in Table 8) was the free space path loss (FSPL). For the LNSP relay-to-Earth link, both FSPL and atmospheric attenuation were considered. For lunar surface-to-surface links, multipath effects were factored into the overall path loss calculation. An achievable data rate for each link was computed by comparing the received power to noise ratio against the required Eb/N0 for the given coding scheme. This analysis focused on the return data direction and assumed that all surface user links would be directed through either the LNSP relays or the SS given that direct visibility to Earth would only be available for at best $\sim$14 days per month at the LSP. Dependent on terrain, some LSP users may have no direct access to the Earth at all.

Results

The link analysis results are summarized in Table 9. This table also describes various multipath loss generation methods for the surface-to-surface links, on top of losses described in Table 8. As a baseline, the first model only includes losses due to FSPL. The next method calculates multipath losses through FEKO and the 5 m resolution DEM of the LSP. Next, we evaluate a 2-ray ground reflection model with the DEM. Finally, we evaluate a worst case rule of thumb for multipath losses: a FSPL calculation but with the link distance raised

Table 8: Communications hardware and link analysis assumptions

	Parameter	Value	Notes and Sources
Surface Station	Transmit Frequency (Ka)	27.25 GHz	SS-to-LNSP (assumed center of the appropriate LunaNet frequency band for all transmit frequencies) [5]
	Transmit Power	20 W	[7]
	Antenna Diameter	1 m	[7]
LNSP Relay Orbiter	Transmit Frequency (Ka)	26.25 GHz	LNSP-to-Earth [5]
	Transmit Power	20 W	[39]
	Antenna Diameter	1 m	[39]
Autonomous Rover	Transmit Frequency (S)	2.245 GHz / 2.2 GHz	Rover-to-SS / Rover-to-LNSP [5]
	Transmit Power	5 W	[40]
	Antenna Diameter (HGA)	0.75 m	[40]
	Antenna Gain (LGA/Omni)	3 dBi	[40]
Astronaut EVA Suit	Transmit Frequency (S)	2.245 GHz / 2.2 GHz	EVA-to-SS / EVA-to-LNSP [5]
	Transmit Power	1 W	[39]
	Antenna Type	Dipole	[39]
Earth Ground Station	Antenna Diameter	18 m	LEGS Antenna [41]
	Lumped Receive Hardware Losses	2 dB	[41]
	System Noise Temperature	240 K	[41]
Shared Assumptions (For all users except Earth Ground Stations)	Lumped Hardware Losses	5 dB	Accounts for circuit losses, pointing losses, polarization losses, etc. (applies on both TX and RX side)
	Antenna Efficiency	55%	[39]
	Eb/N0 Threshold	2.2 dB	Assume LDPC 1024, r=1/2 coding scheme, OQPSK modulation, Acceptable BER of 1e-8 [39]
	System Noise Temperature	600 K	Accounts for internal receiving hardware noise sources and lunar surface hot body noise
	Link Margin	3 dB	Applied to all links

to the power of 4 instead of 2 ("Range^4"). A pessimistic option further increases losses for this worst case model by 10 dB. These multipath models describe a significant range of possible multipath fading. However, it is clear that with nearly all of the multipath models, the communication links through the SS relay are still bandwidth limited rather than power constrained.

Given a modestly sized LNSP relay and a LEGS ground station, the LNSP-Earth link was found to be capable of $\sim$1 Gbps data rate at Ka-band. This performance level is consistent with previous lunar relay studies and the expected performance of LEGS [39][41]. An SS equipped with a 1-meter Ka-band antenna was found to be capable of 1.6 - 4 Gbps to the LNSP when limited by power only, with the range in data rates arising from the variation between the minimum and maximum range between the LSP and a visible lunar relay in a 12-hour ELFO. Due to bandwidth constraints, this link will likely have a maximum data rate of around 1 Gbps regardless of SS-to-LNSP distance. Thus, the performance of the SS-to-LNSP link roughly matches that of the LNSP-Earth trunk link. If desired, the SS could communicate direct-to-Earth with approximately the same throughput as the LNSP relay trunk link (given that the relay and SS were assumed to have the same sized antennas). However, it will often be necessary to go through the LNSP relays due to the lack of continuous access between the LSP and Earth.

Rover User— For the rover user, we assumed a similar telecommunication system to that of the planned Endurance rover [40]. This includes a 75 cm S-band high gain antenna (HGA), as well as an omni-directional S-band low gain antenna (LGA). With the HGA, the rover is capable of communicating at only 1.5 - 3.75 Mbps directly to the LNSP orbiters. However, when communicating to the nearby SS with its omni-directional LGA, the link can achieve on the order of tens to hundreds of Gbps when only power constrained. In reality, these extreme data rates are infeasible due to spectral allocation and efficiency limitations, thus this analysis assumed a bandwidth limited maximum data rate of 300 Mbps. This rate was estimated from the bandwidth allocated for S-band surface-to-surface links in the LNIS of

Table 9: Communication data rates of links between surface users (rover and astronaut during EVA) and the SS relay or the LNSP relay orbiter. All data rates are likely bandwidth limited except for links marked with *; these are power limited.

Link	Band	Range/Path Loss Conditions			Data Rate		
		Min	Avg	Max	Min Loss	Avg Loss	Max Loss
LNSP to Earth	Ka	356,450 km	385,000 km	406,700 km	1.24 Gbps*	1.06 Gbps*	0.95 Gbps*
SS to LNSP	Ka	5240 km	7290 km	8280 km	1 Gbps	1 Gbps	1 Gbps
Rover (HGA) direct to LNSP	S	5240 km	7290 km	8280 km	3.75 Mbps*	1.94 Mbps*	1.50 Mbps*
Rover (LGA) to SS	S	1 km (FSPL, 99.5 dB)	5 km (FSPL, 113.5 dB)	10 km (FSPL, 119.5 dB)	300 Mbps	300 Mbps	300 Mbps
Rover (LGA) to SS	S	1 km (FEKO, 107 dB)	5 km (FEKO, 114 dB)	10 km (FEKO, 120 dB)	300 Mbps	300 Mbps	300 Mbps
Rover (LGA) to SS	S	1 km (2-Ray, 95.3 dB)	5 km (2-Ray, 122 dB)	10 km (2-Ray, 134 dB)	300 Mbps	300 Mbps	300 Mbps
Rover (LGA) to SS	S	1 km (Range^4, 100 dB)	5 km (Range^4, 128 dB)	10 km (Range^4, 140 dB)	300 Mbps	300 Mbps	111 Mbps*
Rover (LGA) to SS	S	1 km (Range^4, 110 dB) (pess)	5 km (Range^4, 138 dB) (pess)	10 km (Range^4, 150 dB) (pess)	300 Mbps	177 Mbps*	11.1 Mbps*
EVA direct to LNSP	S	5240 km	7290 km	8280 km	12.6 kbps*	6.49 kbps*	5.03 kbps*
EVA to SS	S	1 km (FSPL, 99.5 dB)	5 km (FSPL, 113.5 dB)	10 km (FSPL, 119.5 dB)	300 Mbps	300 Mbps	300 Mbps
EVA to SS	S	1 km (FEKO, 107 dB)	5 km (FEKO, 114 dB)	10 km (FEKO, 120 dB)	300 Mbps	300 Mbps	300 Mbps
EVA to SS	S	1 km (2-Ray, 95.3 dB)	5 km (2-Ray, 122 dB)	10 km (2-Ray, 134 dB)	300 Mbps	300 Mbps	122 Mbps*
EVA to SS	S	1 km (Range^4, 100 dB)	5 km (Range^4, 128 dB)	10 km (Range^4, 140 dB)	300 Mbps	300 Mbps	30.6 Mbps*
EVA to SS	S	1 km (Range^4, 110 dB) (pess)	5 km (Range^4, 138 dB) (pess)	10 km (Range^4, 150 dB) (pess)	300 Mbps	48.9 Mbps*	3.06 Mbps*

150 MHz (2.5035 - 2.655 GHz) [5] and the assumption of 2 bits/symbol through QPSK, resulting in a 2 bits/symbol $\times$ 150 MHz = 300 Mbps.

Even with bandwidth limitations, the rover-to-SS link far exceeds the direct rover-to-LNSP relay link in data rate by two orders of magnitude. It is important to note that the improvement in data rate through the rover-to-SS link was achieved while also switching from the rover's directional HGA (which requires precise pointing) to the omni-directional LGA. This demonstrates how the SS can enable higher data rates while also mitigating the SWaP and operational complexity required of future LSP missions.

Astronaut EVA User—The link analysis demonstrates similar improvements for the astronaut EVA suit links. When communicating directly to a LNSP relay, the EVA suit's relatively low power dipole antenna is only capable of 5 - 12 kbps, however, when communicating with the nearby SS, the EVA suit is mostly bandwidth limited at 300 Mbps. Even with the worst case, power constrained multipath loss model (pessimistic "Range^4"), the EVA-to-SS link is capable of 3 Mbps, orders of magnitude larger than the direct link from EVA-to-LNSP relay.

It is clear that an SSE PNT+C architecture provides significant communications benefits for LSP users, especially users that will need to prioritize low SWaP hardware. In addition to data rate benefits, funneling data from multiple local users through the SS simplifies operations for LNSP relays, which would only need to communicate with the SS, rather than each user individually. Although this analysis only evaluates surface-to-surface links up to 10 km in distance, longer range links are possible from a power perspective. Over the horizon communications links may be possible with diffraction effects described in Figure 7.

6. The Moon to Mars Architecture

This analysis mainly focuses on the implementation of an lunar SSE PNT+C architecture to support the early deployment phases of a large lunar constellation. However, the applications of SSE PNT+C extend past the Moon. At its core, SSE PNT+C is a minimal infrastructure communications and navigation architecture. Thus, SSE PNT+C is directly extensible to the development of communication and navigation services at other planetary bodies (Mars, Europa, outer planets, etc), which may only be able to support sparse

infrastructures.

NASA plans to use the lessons learned during the return to the Moon as a stepping stone for future Mars missions through its Moon to Mars Architecture [42]. Thus, this section will briefly analyze the application of an SSE PNT+C architecture at Mars and discuss some important considerations during the Moon to Mars initiative. Table 10 at the end of this paper summarizes the differences in technical and environmental constraints between the Moon and Mars.

Published literature includes various feasibility studies for Mars navigation systems [43] - [45]. Several Martian orbiters currently support communication and navigation for missions in the vicinity and on the surface of Mars. The orbiters in this Mars Relay Network (MRN), are equipped with instruments to relay data between Earth and Mars surface missions, map the Martian surface, and assist in navigation. For instance, the Mars Reconnaissance Orbiter (MRO) serves as a crucial relay for communications between Mars rovers and Earth. MRO, along with the Mars Atmosphere and Volatile EvolutioN (MAVEN) and ExoMars Trace Gas Orbiter (TGO) utilize the Electra UHF radio for these relay services. For navigation, TGO recently demonstrated radiometric navigation of the InSight Lander using 1-way and 2-way Doppler measurements [46]. However, providing navigation services is not the primary function of any of these orbiters. In addition, many of the orbiters in the MRN are past their original mission lifetimes, and will likely not be able to support far future Martian missions. Thus, we assume that for far future Martian missions, there will be a dedicated Martian PNT+C constellation, similar to the LunaNet systems proposed for the Moon.

Some key differences will be in the orbit designs of the Martian PNT+C constellations. ELFO orbits were an attractive choice for lunar constellation initiatives due to the focus on the LSP. ELFOs provide increased coverage and access durations at the LSP at the detriment of reduced access at the rest of the lunar surface. The target region for Mars likely ranges from the northern and southern mid latitudes; a Martian constellation would thus optimize for global longitudinal coverage, up to these mid latitudes. This typically results in circular orbits, likely inclined for improved navigation geometry. These orbiters will likely be in medium Martian orbits to increase coverage, far above the current MRN orbiters which range from 200 - 400 km in altitude. Ultimately, because the constellation does not have a target region to focus on, users may have access to fewer simultaneous relay orbiters for PNT+C needs. This, along with the large cost of deploying a Martian relay constellation, may make the implementation of an SSE PNT+C architecture a necessity for real-time and accurate PNT+C services on the Martian surface.

Without a specific target region on the Martian surface, the location of a potential Martian SS is to be determined. Future missions, such as human Martian missions, will dictate the target regions that require higher PNT+C performance. Crewed missions to Mars will likely follow multiple autonomous landers to the human landing site, all of which would prepare the site for human arrival. One (or more) of these landers could be dedicated for SSE PNT+C services, or SSE payloads could be deployed on multiple landers. As future missions explore more of the Martian surface, the landing component of the missions could provide SSE PNT+C services for nearby surface users.

Navigation accuracy requirements will vary among user types. Mars landers require precise navigation during descent and landing; studies have shown the viability of EDL navigation using radiometric measurements from the Mars Network [44]. Access to an SS during atmospheric entry is not likely during atmospheric braking, but the descent and landing could utilize an SSE system. Astronauts will likely have the most stringent navigation and communication requirements, but they will typically stay within a few kilometers from their habitats. Thus, an SSE payload on the habitat may be a necessity to achieve their stringent PNT+C requirements. Autonomous rovers can range from long distance explorers to short distance utility machines. An example of the latter would be an ISRU rover, which could utilize a central SS for PNT+C services. Long distance rovers will likely be out of reach of SSs, but can still utilize navigation corrections sent through the relay orbiter constellation. These rovers will achieve their navigation requirements with a fusion of measurements, including inertial navigation systems (INS), cameras, and odometry. However, SSE and radiometric measurements still play a critical role in improving absolute and long-term positioning accuracy.

An accurate timing and frequency reference in a Martian SS will be crucial for maintaining timing synchronization of the Martian relay constellation and timekeeping of the Martian coordinated time. The infrequent communications with Earth highlight the benefits for SSE not only for timing but also for in-situ orbit determination.

Finally, there are significant differences in environmental considerations between Mars and the Moon. The largest difference is the Martian atmosphere. Just as on Earth, transmitting pseudorange codes through a charged atmosphere can lead to delays in the signal that result in errors in the range measurement. On Earth, atmospheric delays can be estimated with DGNSS and the corrections relayed to users. Thus, a Martian SS would provide similar corrections for its local region. Temperature ranges on the Martian surface are not as significant as on the LSP, reducing hardware requirements for an SS. With frequent dust storms, a long-term SS will likely require an internal power source, such as an RTG.

Ultimately, a Martian implementation of an SSE PNT+C architecture will require changes from a lunar implementation. However, the benefits of SSE are clear on Mars and, by extension, any other planet with sparse infrastructures.

7. Conclusions and Future Work

The SSE PNT+C architecture provides significant cost savings, time savings, and PNT+C improvements to a near-term lunar constellation. An SS on the LSP provides not only JDR and differential corrections to nearby surface users, but also improved geometric diversity with an additional AFS broadcast. Communications relay through the SS increases data throughput, reduces hardware requirements on all users, and simplifies LNSP network operations. Timekeeping and OD through the SS also reduces burden on the DSN. Applications reach beyond the Moon to Mars and exploratory missions to other planetary bodies.

Future work for SSE PNT+C includes additional lunar orbit design studies, initial designs for small scale SSE payloads, improved navigation and communication simulations, and hardware demonstrations of SSE corrections.

Although this paper mainly discusses a large, dedicated

lander acting as the SS, the SSE objectives may still be possible in a low-SWaP design. An SSE payload could be deployed early through the CLPS program, providing critical services for near-term Cislunar missions with stringent PNT+C requirements, such as the Artemis missions. Thus, we plan to explore designs for an SSE payload and evaluate compromises with the limited SWaP. A future hardware demonstration of SSE PNT+C on Earth using GNSS signals would increase the TRL of SSE PNT+C in preparation for a CLPS payload.

ACKNOWLEDGMENTS

The research was carried out at the Jet Propulsion Laboratory, California Institute of Technology, under a contract with the National Aeronautics and Space Administration (80NM0018D0004).

The authors would like to thank Todd Ely for his helpful conversations related to constellation design.

Pre-Decisional Information – For Planning and Discussion Purposes Only.

REFERENCES

[1] NASA. (2024) Lunar communications relay and navigation systems (lcrns). [Online]. Available: https://tempo.gsfc.nasa.gov/projects/LCRNS

[2] ESA, "Moonlight programme white paper," ESA, Tech. Rep., 2022.

[3] M. Murata, "Lunar navigation satellite system (lnss): Overview, plan, and demonstration mission," JAXA, Tech. Rep., 2023.

[4] NASA and ESA, "Lunanet signal-in-space recommended standard - augmented forward signal (ad1)," National Aeronautics and Space Administration, Tech. Rep., 2023.

[5] ——, "Lunanet interoperablility specification draft version 5," National Aeronautics and Space Administration, Tech. Rep., 2023.

[6] B. Hofmann-Wellenhof, H. Lichtenegger, and E. Wasle, *GNSS - Global Navigation Satellite Systems*. SpringerWienNewYork, 2008.

[7] S. R. Oleson and M. L. McGuire, "Compass final report: Lunar communications terminal (lct)," NASA Glenn Research Center, Cleveland, OH, Tech. Rep., 2010.

[8] M. C. Scardelletti and et al., "Lunar surface network relay terminal: A lunar communications platform," in *International Communications Satellite Systems Conference (ICSSC)*, 2023.

[9] W. W. Jun, K. M. Cheung, E. G. Lightsey, and C. Lee, "A minimal architecture for real-time lunar surface positioning using joint doppler and ranging," *IEEE Transactions on Aerospace and Electronic Systems*, vol. 58, no. 2, pp. 1367–1376, April 2022.

[10] W. W. Jun, K. M. Cheung, and E. G. Lightsey, "Real-time position, velocity, and timing estimation of lunar surface users with joint doppler and ranging," *IEEE Transactions on Aerospace and Electronic Systems*, vol. 60, no. 4, pp. 5525–5537, August 2024.

[11] W. W. Jun, K.-M. Cheung, and E. G. Lightsey, "Position, velocity, and timing for lunar descent and landing with joint doppler and ranging," in *IEEE Aerospace Conference*, Big Sky, MT, 2024.

[12] E. A. Burt and et al., "Demonstration of a trapped-ion atomic clock in space," *Nature*, vol. 595, pp. 43–47, 2021.

[13] T. M. Hoang and et al., "Micro mercury trapped ion clock prototypes with 10-14 frequency stability in 1-liter packages," *Scientific Reports*, vol. 13, 2023.

[14] W. W. Jun, K. M. Cheung, and E. G. Lightsey, "Frequency bias mitigation for surface user navigation using double differencing joint doppler and ranging," *IEEE Transactions on Aerospace and Electronic Systems*, August 2024.

[15] P. Misra and P. Enge, *Global Positioning System: Signals, Measurements, and Performance Revised Second Edition*. Ganga-Jamuna Press, 2012.

[16] T. A. Ely, "Selected orbits of the first two andromeda constellation satellites for use in a parametric study of lunar surface communication and surface positioning," Jet Propulsion Laboratory, Pasadena, CA, Tech. Rep., 2024.

[17] T. A. Ely and et al., "Mars network constellation design drivers and strategies," in *AAS/AIAA Astrodynamics Specialist Conference*, Girdwood, AK, 1999.

[18] T. A. Ely, "Stable constellations of frozen elliptical inclined lunar orbits," *Journal of the Astronautical Sciences*, vol. 53, no. 3, 2005.

[19] T. A. Ely and E. Lieb, "Constellations of elliptical inclined lunar orbits providing polar and global coverage," *Journal of the Astronautical Sciences*, vol. 54, no. 1, 2006.

[20] N. Speciale, "Lunar relay services requirements document (srd)," National Aeronautics and Space Administration, Goddard Space Flight Center, Tech. Rep., 2022.

[21] J. Ventura-Traveset, "Esa lunar navigation plans: Lunar pathfinder & moonlight," International Committee on Global Navigation Satellite Systems, Tech. Rep., 2022.

[22] D. Y. Stodden and J. M. Coggi, *"Space System Architecture Analysis and Wargaming: The Satellite Orbit Analysis Program (SOAP)*. CRC Press, 2024.

[23] S. Evans and et al., "Monte: The next generation of mission design and navigation software," *CEAS Space Journal*, vol. 10, 2018.

[24] R. F. Sunseri and et al., "Mission analysis, operations, and navigation toolkit environment (monte) version 040," Jet Propulsion Laboratory, Pasadena, CA, Tech. Rep., 2012.

[25] F. T. Krogh, "Variable order adams method for ordinary differential equations (diva)," Math 'a la Carte, Tujunga, CA, Tech. Rep., 1975.

[26] ——, "Diva/siva, chapter 14.1 of math77, release 4.0," Jet Propulsion Laboratory, Pasadena, CA, Tech. Rep., 1992.

[27] R. S. Park, W. M. Folkner, J. G. Williams, and D. H. Boggs, "The jpl planetary and lunar ephemerides de440 and de441," *The Astronomical Journal*, vol. 161, no. 3, 2021.

[28] J. E. Gruener and et al., "Shackleton - de gerlache ridge: A strong candidate for important lunar science, science

opeartions, and polar volatiles," in *Lunar Surface Science Workshop 2020 (LPI Contrib. No. 2241)*, 2020.

[29] NASA. (2024) Planetary data sysem: Lro: Lola. [Online]. Available: https://pds-geosciences.wustl.edu/missions/lro/lola.htm

[30] QGIS. (2024). [Online]. Available: https://www.qgis.org/

[31] Altair, "Altair feko," 2024. [Online]. Available: https://altair.com/feko

[32] H. Williams and et al., "Lunar array, mast, and power system (lamps) for deployable lunar power provisions," in *AIAA SCITECH 2023 Forum*, 2023.

[33] A. S. Miller and et al., "Design development of a stable, lightweight, tall and self-deploying lunar tower," in *IEEE Aerospace Conference*, Big Sky, MT, 2023.

[34] P. Gläser, A. Sanin, J.-P. Williams, I. Mitrofanov, and J. Oberst, "Temperatures near the lunar poles and their correlation with hydrogen predicted by lend," *Journal of Geophysical Research: Planets*, vol. 126, no. 9, 2021.

[35] NASA, "Multi-mission radioisotope thermoelectric generator (mmrtg)," NASA Facts, NF-2020-05-619-HQ, Tech. Rep., 2020.

[36] K. Sherick and et al., "Development of a small-low power radioisotope thermoelectric generator using the general purpose heat source," in *IEEE Aerospace Conference*, Big Sky, MT, 2024.

[37] A. Grenier, P. Giordano, L. Bucci, A. Cropp, P. Zoccaranto, R. Swinden, and J. Ventura-Traveset, "Positioning and velocity performance levels for a lunar lander using a dedicated lunar communication and navigation system," *NAVIGATION: Journal of the Institute of Navigation*, vol. 69, no. 2, 2022.

[38] E. Kaplan and C. Hegarty, *Understanding GPS/GNSS: Principles and Applications*. Artech House, 2017.

[39] S. R. Oleson and M. L. McGuire, "Compass final report: Lunar network satellite-high rate (lns-hr)," NASA Glenn Research Center, Cleveland, OH, Tech. Rep., 2012.

[40] J. T. Keane, S. M. Tikoo, and J. Elliot, "Endurance: Lunar south pole-aitken basin traverse and sample return rover - mission concept study report," NASA, Tech. Rep., 2023.

[41] SCaN, "Space communications and navigation (scan) lunar exploration ground sites (legs) brochure," NASA, Tech. Rep., 2023.

[42] NASA, "Moon to mars architecture definition document," NASA Exploration Systems Development Mission Directorate, ESDMD-001 Rev A, Tech. Rep., 2023.

[43] K.-M. Cheung and C. Lee, "In-situ navigation and timing services for the human mars landing site part 1: System concept," in *International Astronautical Congress*, Adelaide, Australia, 2017.

[44] E. G. Lightsey, A. E. Mogensen, P. D. Burkhart, T. A. Ely, and C. Duncan, "Real-time navigation for mars missions using the mars network," *Journal of Spacecraft and Rockets*, vol. 45, no. 3, 2008.

[45] T. A. Ely and J. Guinn, "Mars approach navigation using mars network based doppler tracking," in *AIAA/AAS Astrodynamics Specialist Conference and Exhibit*, Monterey, CA, 2002.

[46] H. Elliott, T. A. Ely, A. Lazaro, E. Gustafson, R. Mendoza, and R. Gladden, "Spacecraft position determination with the electra uhf transceiver: A comparison of one-way and two-way doppler observations," in *IEEE Aerospace Conference*, Big Sky, MT, 2024.

BIOGRAPHY

William Jun *received his B.S., M.S., and Ph.D. degrees in aerospace engineering from the Georgia Institute of Technology in Atlanta, Georgia in 2018, 2020, and 2023 respectively. He is currently a Telecommunications Engineer at NASA Jet Propulsion Laboratory (JPL). During his stay at Georgia Tech, he worked in the Space Systems Design Laboratory (SSDL) on various CubeSat missions as subsystem leads and as the Project Manager of Prox-1. He was a Research Fellow at NASA JPL in the summers of 2018 to 2023. His research interests include navigation architectures, navigation methods, and estimation techniques. He was a recipient of the NASA Space Technology Research Fellowship in 2019 and the M. Charles Fogg Best Paper Award at the 2024 IEEE Aerospace Conference.*

Toshiki Tanaka *received his Ph.D. in Electrical and Computer Engineering from the University of Houston, earned in 2023 with a dissertation award. He also holds M.S. and B.S. degrees in Aeronautics and Astronautics Engineering from the University of Tokyo, received in 2010 and 2008, respectively. Since 2023, Toshiki has been a space and robotic systems engineer in the Section 337 Flight Communication Group at the Jet Propulsion Laboratory, where he provides systems engineering support for the development of flight telecom systems and transponders. Additionally, he is engaged in research and technology development (R&TD) for lunar navigation satellite architecture. Toshiki's research interests include spacecraft systems design, machine learning-based robotics guidance, navigation and control, as well as positioning, navigation, timing, and communication systems for the Moon and interplanetary missions.*

Paul Carter *received his B.S. and M.S. degrees in Aerospace Engineering from the Georgia Institute of Technology in 2021 and 2023 respectively. During both his undergraduate and graduate years, he was a member of the Georgia Tech Space Systems Design Laboratory (SSDL). While there, he worked on CubeSat missions and started his research on deep space relay architectures. He is now working full time as a Telecommunications Engineer at NASA Jet Propulsion Laboratory (JPL).*

Sriramya Bhamidipati *received her Ph.D. in Aerospace Engineering at the University of Illinois, Urbana-Champaign in 2021, where she also received her M.S in 2017. She obtained her B.Tech. in Aerospace from the Indian Institute of Technology, Bombay in 2015. She is currently a robotics technologist in the maritime and multi-agent autonomy group at NASA JPL. Her research interests include GPS, computer vision, unmanned aerial vehicles and space robotics. Before joining JPL, she worked as a postdoctoral scholar in the navigation and autonomous vehicles lab at Stanford University. She received the Amelia Earhart Fellowship in 2020 and was awarded best presentation at ION GNSS+ four times in 2016, 2017, 2021 and 2022.*

Rodney L. Anderson *received his Ph.D. and M.S. in Aerospace Engineering Sciences from the University of Colorado at Boulder and his Bachelor's degree from North Carolina State University. He is currently a Technologist in the Mission Design and Navigation section at the Jet Propulsion Laboratory, California Institute of Technology where he has worked since 2010. He has been a PI on multiple research tasks focused on applying dynamical systems techniques to solving astrodynamics problems, and he is a recipient of JPL's Lew Allen award. His research interests are focused on astrodynamics, mission design, machine learning, navigation, and celestial mechanics.*

Kar-Ming Cheung *received the B.S.E.E. degree from the University of Michigan, Ann Arbor, in 1984, and the M.S. and Ph.D. degrees from California Institute of Technology in 1985 and 1987, respectively. He is a Principal Engineer and Technical Group Supervisor in the Communication Architectures and Research Section (332) at JPL. His group supports design and specification of future deep-space and near-Earth communication systems and architectures. Since 1987, he has been with JPL where he is involved in research, development, production, operation, and management of advanced channel coding, source coding, synchronization, image restoration, and communication analysis schemes. Dr. Cheung received NASA's Exceptional Service Medal for his work on Galileo's onboard image compression scheme.*

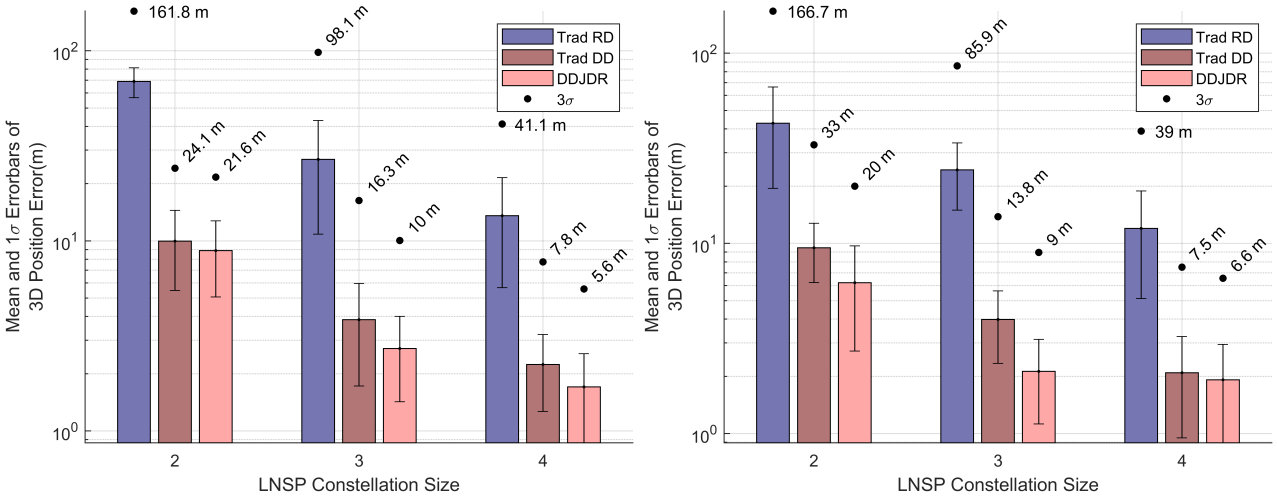

(a) Crewed vehicle: circular trajectory

(b) Autonomous rover: grid trajectory

Figure 17: Mean (bars), 1σ (error bars), and 3σ (points) of positioning error for all methods and both user types.

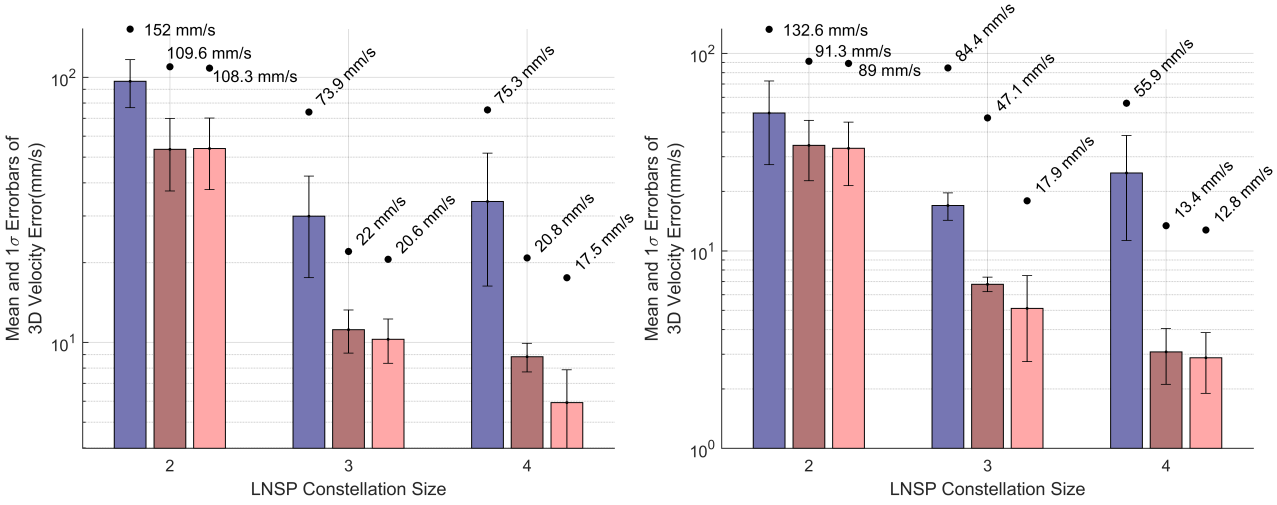

(a) Crewed vehicle: circular trajectory

(b) Autonomous rover: grid trajectory

Figure 18: Mean (bars), 1σ (error bars), and 3σ (points) of velocity error for all methods and both user types.

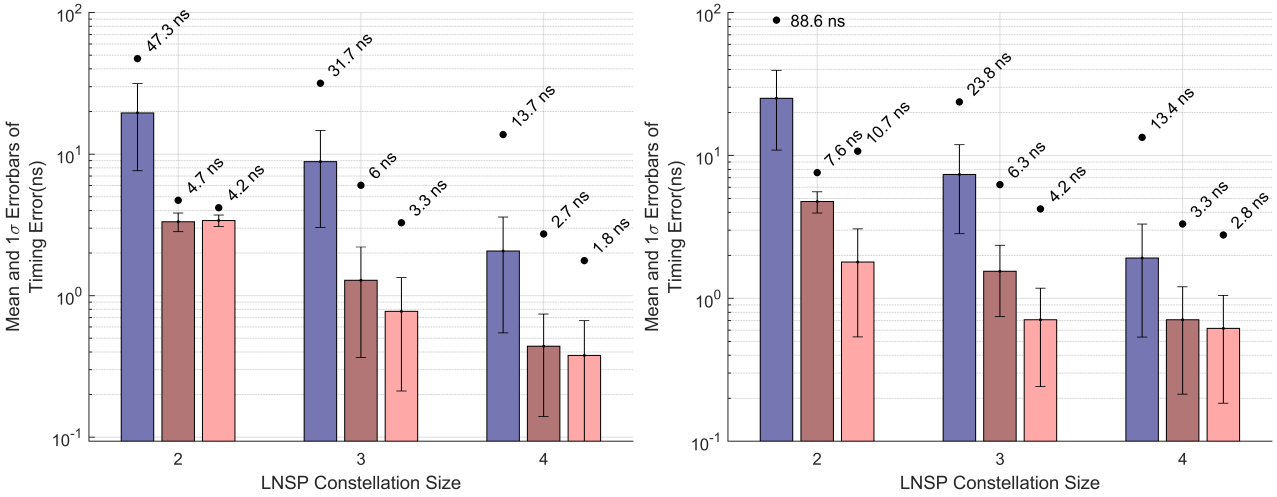

(a) Crewed vehicle: circular trajectory

(b) Autonomous rover: grid trajectory

Figure 19: Mean (bars), 1σ (error bars), and 3σ (points) of timing error for all methods and both user types.

Table 10: Key differences in technical and environmental constraints for an SS deployed on the Moon or on Mars.

Item	Moon Surface	Mars Surface	Design Impact
Service target regions	Lunar south pole	No specific landing sites. Landing sites for manned missions will likely be within the mid latitudes.	Affects the number and location of surface stations.
Line of sight to Earth	Moon occultation results in lack of Earth access of the station for $\sim$14 days at south pole.	Line of sight from Mars to Earth only lasts a few hours per day.	Affects autonomy requirements for the station and users.
Distance to Earth	363,300 km - 405,500 km	54.6 M km - 401 M km	Affects station to Earth communication hardware sizing
Direct-to-Earth signal travel time	1.5 sec	4.3 min – 22 min	Lack of real-time communication may lead to increased needs for autonomous rover positioning/exploration capabilities.
Distance between orbiters and surface users/station	Lunar south pole to ELFOs 5,800 km - 8,300 km	Current orbiters: 250 km – 400 km (MRO), 400 km (TGO) Future orbiters: medium Mars orbit	Affects transmission power from SS to orbiters and surface users to orbiters.
GNSS weak signal availability	Likely yes	No	Orbit determination of Martian orbiters will need to rely on Earth and Martian ground stations. Both lunar and Martian SS will likely utitize orbiters for precise positioning.
Ionospheric effects	No	The Martian ionosphere affects low-frequency waves (less than 450 MHz)	The ionosphere can potentially be used for Mars surface trans-horizon communication. When a high-speed spacecraft enters the Martian atmosphere, a plasma sheath is formed in the front of the spacecraft due to the impacting ionization. This can cause a communication blackout. The Martian SS can provide PNT+C services before and after these blackouts.
Tropospheric effects	No	Negligible	
Optical communications visibility to Earth	Yes	No	Optical communications between a Martian SS and Earth is likely not feasible.
Dust storms	No	Yes	Affects short-term communication performance on the surface. May require dust removal for solar panels.
Length of a day	28 days	24 hr 39 min	Affects SS thermal/power systems design
Angle of incident sunlight	0 - a few degrees at South pole	0 - 90 degrees	Affects SS thermal/power systems design
Atmospheric pressure	0	6 to 7 millibars	Affects SS thermal/power systems design
Surface temperature	-200 C to +50 C at south pole, depending on the topography	-130 C to +30 C	Affects SS thermal/power systems design
Surface gravity	1.6 m/s^2	3.71 m/s^2	Affects in-situ tower deployment design